Chem Soc Rev

REVIEW ARTICLE

View Article Online
View Journal | View Issue

Cite this: *Chem. Soc. Rev.*, 2018, **47**, 2485

Imaging the chemical activity of single nanoparticles with optical microscopy

Wei Wang

Nanomaterials exhibit structural and functional heterogeneity among individual nanoparticles, thus requiring a capability to study single nanoparticles. While electron microscopes often provide static images of their chemical composition, morphology and structure, imaging the chemical activity of single nanoparticles is highly desirable for exploring the structure–activity relationship *via* a bottom-up strategy, to understand their microscopic reaction mechanisms and kinetics, and to identify a minority subpopulation with extraordinary activity. Recently, various optical microscopes have been emerging as powerful techniques towards this goal, owing to their non-invasive nature, excellent sensitivity, diversified spectroscopic principles and sufficient spatial and temporal resolution. In this review, we first introduce the motivational concept and the strength of using optical microscopy to study the chemical activity of single nanoparticles. In the second section, five types of commonly used optical microscopy, fluorescence microscopy, dark-field microscopy, surface plasmon resonance microscopy, Raman microscopy and photothermal microscopy are described, with an emphasis on their applicable nanomaterials and mechanisms for application. Recent achievements of these techniques in nanosensing, nanoelectrochemistry and nanocatalysis are surveyed and summarized in the subsequent sections, respectively. We finally conclude with our perspective on the remaining challenges and the future trends in this field.

Received 1st January 2018

DOI: 10.1039/c7cs00451f

rsc.li/chem-soc-rev

State Key Laboratory of Analytical Chemistry for Life Science, School of Chemistry and Chemical Engineering, Nanjing University, Nanjing 210023, China.
E-mail: wei.wang@nju.edu.cn; Tel: +86-25-89682185

Wei Wang

Wei Wang is a Professor at Nanjing University. He received his BS in 2004 and PhD in 2009, both from the University of Science and Technology of China (USTC). He pursued postdoctoral studies with Prof. Nongjian Tao at Arizona State University from 2009 to 2013 before joining the faculty of Nanjing University in December 2013. He received support from the Thousand Young Talents Program (2013) and the National Natural Science Foundation of China for Excellent Young Scholars (2015). He also received the Young Chemist Award from the Chinese Chemical Society in 2017. His current researches involve advanced optical microscopy for single-cell imaging, nanoelectrochemistry, and single-molecule detection.

Introductions

Various chemical activities of nanomaterials enable their exciting application in broad fields ranging from clean energy and heterogeneous catalysis to chemical and bio-sensing. One of the most intrinsic features associated with nanomaterials is the structural and functional heterogeneity among individual nanoparticles. Each nanoparticle is structurally different from all others in terms of chemical composition, morphology, atomic arrangement, lattice defects and surface chemistry, leading to dramatically different activities when involved in chemical processes. Ensemble measurements (both structural characterizations and activity determinations) only provide averaged results of billions of nanoparticles, which blur the structure–activity relationship and are likely to overlook a minority subpopulation with outstanding activity. In order to draw a microscopic picture of nanomaterials, the capability of studying single nanoparticles is of particular interest as it can access these heterogeneities. While structural characterizations of single nanoparticles have become routine in materials science with the help of electron microscopes, interrogating chemical activity (function) at the single-nanoparticle level has proven to be a more challenging task. This is because chemical environments, such as solvents, reactants and electrolytes, play essential roles in regulating the chemical activity. They are often not compatible with the

vacuum conditions and high-energy beam in electron microscopes, despite recent developments in liquid-cell and *in situ* electron microscopy.

The optical microscope is the earliest design of microscope for magnifying and resolving tiny objects based on light–matter interactions. In contrast to the centuries-long history of routinely using optical microscopes in biological labs, however, their application in nanoscience and molecular science has been part of a new wave since the 1990s when fluorescence microscopy (FLM) demonstrated its capability of studying single organic molecules[1] and CdSe quantum dots.[2] Since then, more types of optical microscopes have been developed and employed to image a broad range of nanomaterials. These include dark-field microscopy (DFM)[3] and Raman microscopy[4] for plasmonic nanomaterials, photothermal microscopy (PTM) for light-absorbing nanomaterials,[5] and surface plasmon resonance microscopy (SPRM) for dielectric and soft nanomaterials,[6] to name just a few. The rapid growth and bright future of using optical microscopes to image chemical activity at the single-nanoparticle level are promised by several strengths, including good environmental compatibility, excellent sensitivity, diversified spectroscopic principles and sufficient spatial and temporal resolution. Because optical microscopes utilize gentle visible light to illuminate the sample, they usually cause subtle, if any, disturbance to the reaction system during measurement. They are satisfactorily compatible with common solvents and reactants. Flow control as well as temperature and pressure control can also be feasibly achieved if necessary.[7] Several kinds of optical microscopes have demonstrated unprecedented sensitivity to detect individual small molecules,[8] substantially paving the way towards single-molecule chemistry.[9] Most importantly, versatile optical and spectroscopic principles and techniques focus on comprehensive aspects of the chemical and electronic structures of nanomaterials, providing rich and essential information for understanding the chemical processes occurring at nanometer-sized scales.

A brief scenario for the chemical imaging of single nanoparticles with optical microscopy is described in Fig. 1. A particular type of optical microscope monitors the corresponding optical signal of single nanoparticles located in an appropriate reaction environment. During continuous recording of optical images, an external stimulus is applied at a certain moment to trigger a chemical reaction, leading to an alteration in optical intensity in a series of time-lapsed images. Common stimuli include the introduction of reactants, and illumination with light, as well as the application of a potential. The chemical activity of each and every individual particle in the field of view can thus be extracted from the corresponding signal traces by virtue of a pre-established optical-to-chemical information conversion model. Then, the sample is characterized with other techniques (such as electron microscopy) to access the structural information of the very same nanoparticles, so that the activity (from the optical microscope) and the structure (from the electron microscope) can be correlated at the single-nanoparticle and even sub-nanoparticle level.

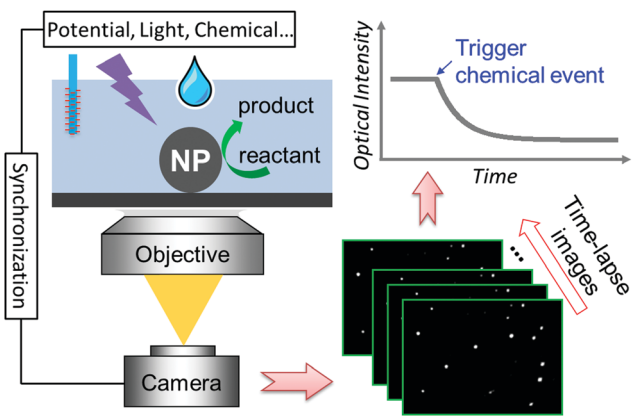

Fig. 1 Schematic illustration of the basic methodology of using optical microscopy to investigate the chemical activity of single nanoparticles.

Existing studies have demonstrated several promising strengths of such an approach. First, it provides a bottom-up strategy to build the structure–activity relationship by correlating the activity and the structure of the very same individuals. Because both the single-nanoparticle structure and the activity can be accurately determined, one can uncover important dependencies of activity on the structural features. For instance, by optically watching the location of products in a fluorogenic reaction catalyzed by a layered double hydroxide crystal, it was found that ester hydrolysis preferentially took place on the lateral [1010] crystal facet while transesterification did not display a facet preference.[10] In addition, hole–electron separation is a critical step for efficient semiconductor photocatalysis. While it has commonly been suggested that electron-assisted reduction reactions and hole-assisted oxidation reactions take place at different sites, Chen *et al.* observed spatial co-localizations between these two competing pathways.[11] Mapping the reactive sites within a single nanoparticle offers a convenient and powerful possibility of accessing these structural preferences that could otherwise be blurred in ensemble methods. Second, it allows for the identification of a minority subpopulation (or even individuals) with extraordinary activity, whose contribution could be overlooked in ensemble measurements. Existing studies have shown significant particle-to-particle variations in surface-enhanced Raman scattering because the enhancement factor is extremely sensitive to the nano-scaled geometry (hot spots) of different individuals. Optical microscopy allows for the determination of the sub-nanoparticle distribution of hot spots,[12] so that one can choose a particular individual with the best Raman enhancement factor for further sensing and chemical applications.[4] Third, it uncovers some mechanistic and kinetic features that are only observable at the single-entity level. A typical example is the intermittent fluorescence emission (photoblinking) from a single fluorophore,[2,13] which has greatly advanced the fundamental understanding of photophysics[14] and has inspired super-resolved FLM.[15,16] A recent study reported the photochemical counterpart of such intermittency by monitoring the photocatalytic hydrogen evolution rate at a single-nanoparticle level.[17] The memory effect in single-molecule enzymatic kinetics[18] and fluctuating activity in single-nanoparticle

catalysis[19] are further examples. Because these behaviors are highly unsynchronized among individual particles, such dynamic characteristics are completely washed out in ensemble experiments, underscoring the unique value of chemical measurements at the single-entity level.

The scope of this review is restricted by three keywords: optical microscopy, chemical activity and nanomaterials. Despite the exciting progress recently achieved by electron microscopy and scanning probe microscopy (including near-field scanning optical microscopes) for studying nano-scaled reactions,[20–24] they are not covered here due to space limitations. For the same reason, we exclude numerous studies that use nanoprobes to detect, locate and track biomolecules in living cells and tissues.[25–27] Instead, we focus on *in vitro* chemical and bio-sensing that emphasize the structural dependence of analytical performance. Single-molecule biophysics[28] and chemistry[9,29,30] are included only when the chemical activity of single nanomaterials is involved. This review is organized as follows. We first introduce the motivational concept and the strength of chemical imaging at the single-nanoparticle level. In the second section, the principle, apparatus, applicable nanomaterials, and mechanisms for the application of several kinds of optical microscopes are described, with an emphasis on their technological development. Because the principle and instrumentation of optical microscopy for chemical imaging are not fundamentally different from those for bio-imaging, which have been well-documented in review papers and textbooks elsewhere,[31,32] here we emphasize the applicable types of nanomaterials, as well as the available mechanisms for chemical applications. The principles and apparatus are only briefly introduced and compared with each other for content integrity and to provide a better understanding of the mechanisms for applications. In the next sections, three major application fields, nanosensing, nanoelectrochemistry and nanocatalysis, are respectively summarized. As this review does not aim to cover all the achievements that have been made in this rapidly growing field, only those milestones and most recent results are selected. A list of existing references is provided for readers who are interested in a more comprehensive survey of the particular subject. We finally provide our perspective on the potentials and challenges, and point out future trends.

Advanced optical microscopy techniques

Two terms, signal-to-background ratio (SBR) and point spread function (PSF), should first be explained before we introduce specific techniques. SBR, *i.e.*, visibility, describes the capability of distinguishing an object from its surrounding background. Whether an optical microscope can see an individual nanoparticle or not is determined by its visibility rather than the resolution. The latter describes the capability of distinguishing an object from an adjacent one. Pushing the limit of resolution is continuously pursued but it is not necessarily required for single-nanoparticle imaging. For example, seeing a 5 nm CdSe quantum dot (QD) can be feasibly achieved under an FLM with regular resolution of around $\sim$300 nm. As long as (1) this nanoparticle is sufficiently far apart from any other nanoparticle by a few microns, and (2) it is bright enough to be identified from the optical background, one can see this nanoparticle and trace its optical signal quantitatively. However, the nanoparticle may not display its real size and morphology in the captured image. Instead, an identical pattern, namely the point spread function (PSF), shows up for all nanoparticles regardless of their size, morphology or even chemical identification, as long as it is smaller than the diffraction limit. The PSF defines the spatial pattern in the image plane of an infinitesimally small spot and it is determined by the particular optical system. A PSF with an intensity distribution following a 2-dimensional Gaussian function is the most commonly encountered because of the diffraction of light (Airy disk). In order to avoid overlapping PSFs, individual nanoparticles are typically immobilized on the substrate at a rather low density to ensure that adjacent nanoparticles are at least as far apart as the size of the PSF.

Fluorescence microscopy (FLM)

Fluorescence (FL) is light emission accompanied by radiative relaxation when a substance in an excited state returns to its ground state. Except for a few examples, such as multiple-photon excitation, FL emission usually has a longer wavelength than the excitation light. Because many types of nanomaterials and molecules exhibit a rather high FL quantum yield and the background scattering can be effectively filtered out by using optical filters, FLM was the earliest and most commonly used optical microscope for imaging single nanoparticles with excellent SBR. The 1990s witnessed the great achievements of FLM in visualizing single organic fluorophores,[1] fluorescent proteins[13] and conjugated polymer molecules.[33] CdSe nanocrystals were the first kind of nanomaterial that was imaged by FLM at the single-entity level.[2] Since then, FLM has demonstrated its strength for investigating the fundamental photophysics as well as the chemical activity of many different types of FL nanomaterials, including up-conversion nanomaterials,[34–36] perovskite QDs,[37–39] polymer dots,[40,41] carbon nanotubes and dots,[42–44] metal nanoclusters[45–47] and relatively large plasmonic metal nanoparticles.[48–50] Nanomaterials exhibit several advantages over molecules for FL imaging, such as a large absorption cross-section, long lifetime, large Stokes shift, improved photostability and a structure-dependent spectrum. So far, several kinds of FL mechanisms have been proposed, including electronic bandgap emission,[51] surface defect-relevant emission[52] and radiative damping of the plasmon resonance of metallic nanostructures.[48] Strictly speaking, photo-luminescence (PL) is a more suitable term for semiconductor and plasmonic nanomaterials because their emission mechanisms are somewhat different from that of conventional molecular FL. To simplify the descriptions, however, this review does not distinguish between these two terms, as they share the same apparatus and mechanisms for applications.

Although the relatively large absorption cross-section of nanomaterials facilitates FL imaging, advanced FLMs are often

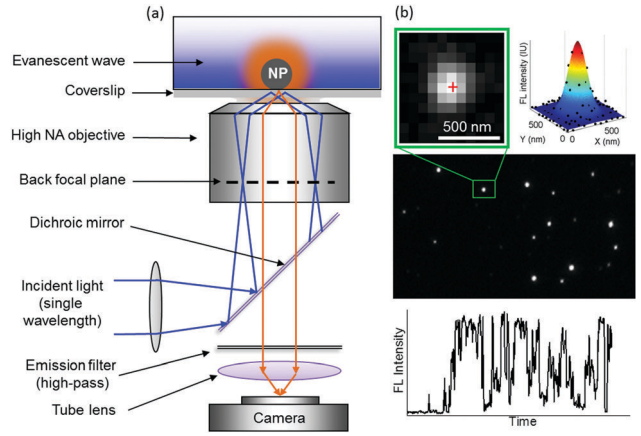

Fig. 2 (a) Representative optical configuration of a TIRFM. (b) Time-lapsed FLM images of single CdSe nanoparticles (middle panel) allow for spatial super-localization analysis of each individual (top panel) and its temporal trajectory (bottom panel).

required to achieve better SBR, especially when the quantum yield is low or the nanoparticle is small. Confocal microscopy and total internal reflection fluorescence microscopy (TIRFM) are two representative configurations for point-scanning and wide-field imaging, respectively. While confocal microscopes are more frequently chosen for thick biological samples, TIRFM is preferred for imaging single nanoparticles that are sparsely distributed on the substrate.[32] Fig. 2a illustrates the representative optical configuration of an objective-based TIRFM. Individual nanoparticles are firmly and sparsely immobilized on the glass coverslip by virtue of electrostatic interaction or van de Waals forces. A monochromatic laser beam is collimated and focused at the back focal plane of an objective with a high numerical aperture (typically 1.4 or above), resulting in a parallel beam of light towards the sample with an adjustable incident angle. When the angle is tuned to be higher than the critical angle at the glass–solution interface, total internal reflection occurs and creates an evanescent wave that penetrates vertically into the solution by a distance much shorter than the wavelength (100–200 nm). The evanescent wave excites the FL emission from the surface-bound nanoparticles, which is collected by the same objective to produce an image in the camera. Since only a very thin layer of solvent receives excitation due to the near-field nature of the evanescent wave, the background scattering is significantly reduced. A dichroic mirror and emission filter further improve the SBR by filtering out the background scattering. Fig. 1b (middle panel) shows a typical FL image of CdSe QDs. Because of the diffraction, photons emitted from single QDs form a blurred dot, which represents the 2-dimensional PSF. Although the full width at half maximum (FWHM) value of the PSF usually ranges from 200 to 300 nm, a super-localization strategy fitting the dot with a 2-dimensional Gaussian function allows one to determine the location of single fluorophores with an accuracy of up to 1 nm (top panel in Fig. 1b).[53] Note that TIRFM is a wide-field imaging technique without the need for laser-scanning. The whole image is acquired within a single exposure time ranging from several milliseconds to hundreds of milliseconds. In addition to objective-based TIRFM, an evanescent wave can also be generated by placing a triangle prism on top of the microscope objective.[19] In this case, the generation of an evanescent wave and the detection of emitted light are achieved by the prism and the objective, which are placed above and below the sample, respectively.

When looking at the representative FL intensity trajectory of single QDs as a function of time (Fig. 1b, bottom panel), an obvious intermittency immediately comes to our attention.[2,54] The FL intensity rapidly and stochastically switches between ON and OFF states, following an empirical power-law distribution.[55] This phenomenon is also known as FL photoblinking, and has been observed in many types of FL nanomaterials.[39,56–58] Although the comprehensive mechanism remains under discussion,[54] it has now become an important criterion by which to determine whether the emitter is a single fluorophore or not. The FL photoblinking has two faces, causing both pros and cons for its applications. For instance, when developing QD-based photovoltaic and display devices, non-blinking nanomaterials are generally desirable to improve the energy conversion efficiency. Blinking is also harmful when using QDs as nanoprobes to label and to trace host proteins in biological samples.[59] However, intermittent emission from single fluorophores is beneficial for developing a super-resolved FL imaging technique.[15,16] In addition, quantitative analysis of the intermittency patterns could reveal important information about the physical and chemical states of the fluorophore.[60]

Mechanisms for applications generally fall into three categories: intensity (enhancement, quenching or blinking), spectrum (wavelength, lifetime and anisotropy), and spatial super-localization. The FL intensity of single emitters is largely influenced by their own chemical states as well as the local nano-photonic environments, resulting in intensity enhancement or quenching, and altered photoblinking patterns. FL emission is found to be greatly enhanced by up to one thousand times when the emitter is close to the hot spots in plasmonic nanostructures.[61–63] The hot spot acts as an optical antenna to amplify the electromagnetic field in the extremely confined vicinity. In addition to plasmonic nanostructures, dielectric environments, such as photonic crystals[64] and silicon nanogaps,[65] were recently found to enhance FL intensity. Such enhancement is sometimes accompanied by a shortened lifetime as well as the altered photoblinking pattern.[66,67] Mapping the super-localization of multiple molecules with enhanced FL intensity allows for the interrogation of the electromagnetic field distribution in this hot spot.[68–70]

Dark-field microscopy (DFM)

The image contrast in DFM comes from the elastic scattering of light by nanoparticles. Oblique illumination keeps the incident light from entering the objective, causing a dark background, as shown in Fig. 3a. Elastic scattering by nanoparticles on the substrate re-emits photons at all angles. Part is collected by the objective to generate a bright dot in the DFM image. However, because the signal (scattered photons from the nanoparticles)

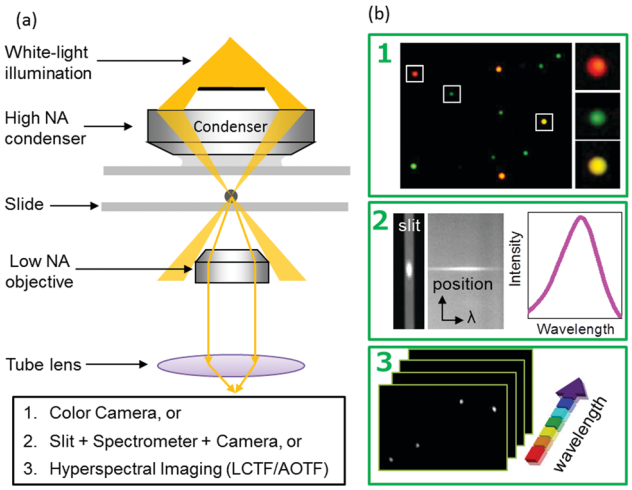

Fig. 3 (a) Representative optical configuration of a conventional DFM. (b) Spectral analysis is achieved by a color camera (top panel), the combination of a slit, a spectrometer and a monochromatic camera (middle panel), or a hyperspectral camera (bottom panel).

and background (scattered photons from solvent and substrates) have the same wavelength, an optical filter is not applicable. Because the Rayleigh scattering cross-section drops with decreasing particle diameter to the power of six, the SBR in DFM is often worse than that in FLM for smaller nanomaterials. In addition, the elastic scattering spectrum lacks the characteristic peaks that are associated with the chemical identity of dielectric nanomaterials.

DFM was not widely utilized for imaging single nanoparticles until 2000 when the scattering spectrum of single 80 nm silver nanoparticles was acquired with a common DFM coupled with a spectrometer.[3] This demonstrated the value of using plasmonic nanoparticles as nanoprobes for sensing and imaging due to the localized surface plasmon resonance (LSPR) effect. The LSPR effect not only enhances the scattering cross-section of nanoparticle to achieve a good SBR, but also enables versatile mechanisms for applications based on characteristic plasmonic bands.[71] Conventional DFM is suitable for imaging plasmonic nanoparticles larger than 30 nm in routine experiments. The literature also demonstrates the direct imaging of gold nanoparticle as small as 10 nm with innovative optical configurations.[72] In addition to metallic nanomaterials, doping semiconductor nanomaterials with charged impurities is able to greatly improve the carrier density and shift their LSPR bands towards a shorter wavelength for DFM observations.[73] More importantly, the scattering spectrum is very sensitive to the morphology and electron density of the nanoparticle itself (internal factor), and the refractive index of the surface adsorbates and surrounding medium (external factor). Such a spectral dependence together with excellent photostability are the major strengths of DFM compared with FLM, allowing for versatile mechanisms for plasmonic probes to sense local chemical information and to report it using the spectral shift.[74] Based on the spectral dependence on the size and morphology, the growth[75,76] and etching[77,78] kinetics of single nanoparticles can be resolved. Electrochemical[79,80] and chemical[81,82] charging are also found to induce a spectral shift although the size and morphology do not change, because the dielectric constant of a plasmonic nanomaterial is a function of its electron density. In addition to these internal factors, the sensitive dependence of the LSPR band on the molecular recognition events occurring on single plasmonic nanoparticles can be utilized to develop nanosensors.[71]

Because spectral information plays a critical role in applications, major instrumentation efforts are made to improve the performance of acquiring the scattering spectrum. The simplest approach is to use a commercial color camera to directly capture the scattering light from the objective (top panel in Fig. 3b). The spectral shift can be roughly estimated by analyzing the RGB channels of the color image.[83–86] For example, when the scattering band shifts from green to red, one can simultaneously detect decreased intensity in the G channel and increased intensity in the R channel. Although a color camera is convenient, it has limited spectral resolution and sensitivity. A grating-based spectrometer coupled with a monochromatic camera is one of the most popular configurations (middle panel in Fig. 3b). A slit is placed at the image plane to select a columnar region-of-interest (ROI), which contains at least one nanoparticle. The slit selectively allows the light inside the ROI to enter into the spectrometer. Dispersed light is subsequently collected by the camera to form a gray-scaled image, in which the horizontal axis represents the wavelength and the vertical axis represents the spatial coordinate along the slit. The spectrum of the single nanoparticle is retrieved by plotting the intensity profile along the wavelength dimension at the position of this nanoparticle. The major drawback of this approach is the throughput. Multiple nanoparticles must be located in the same columnar ROI in order to collect their spectra simultaneously. A diffraction grating with reduced groove density allows for the simultaneous capture of the zeroth-order and 1st-order streaks of multiple nanoparticles.[87,88] The reduced spectral resolution results in an increased throughput. Optimized spectral resolution and throughput can be further achieved with a hyper-spectral camera (bottom panel in Fig. 3b), which utilizes electro-optical devices (such as liquid-crystal and acousto-optic tunable filters) to allow the passage of light based on its wavelength.[89–92] By scanning the voltage of the electro-optical device (equivalent to a wavelength scan) and correlating the wavelength with the camera response, a series of time-lapsed DFM images provide comprehensive spectra of all nanoparticles in the image. In this case, improved throughput is compromised by the limited spectral resolution (electro-optical devices) and the reduced temporal resolution due to voltage (wavelength) scanning.

For those applications that require very high temporal resolution, monochromic DFM is an alternative choice.[80,93,94] Such a design does not provide the original (static) spectrum. Instead, it converts the spectral shift to an intensity change by applying monochromatic light illumination. Therefore, it is mostly suitable for studying dynamic systems with rapid kinetics. Usually, the wavelength corresponding to the largest stiffness in the original spectrum is selected to achieve the highest sensitivity.

In addition to the spectrum acquiring unit, the light source and illumination configuration can also be optimized to achieve a better SBR. For instance, several recent reports have suggested the adoption of a super-continuum white laser instead of the commonly used halogen lamp, mercury lamp or xenon lamp.[72,95–97] An evanescent wave was also utilized to illuminate the nanoparticles, leading to reduced background and polarized excitation to resolve the orientation of anisotropic nanorods.[97–101]

Surface plasmon resonance microscopy (SPRM)

SPR is the resonant oscillation of conduction electrons occurring at a planar metal–dielectric interface under particular light excitation.[102,103] Unlike the LSPR effect where the collective oscillation of free electrons is often localized in a very confined interfacial region (a few nanometers), the planar SPR effect relies on the propagation of surface plasmon polaritons (SPPs) along a planar interface by a much longer distance, ranging from several microns to tens of microns. When looking at the direction perpendicular to the interface, SPPs penetrate into the dielectric layer with an exponentially decreased intensity as a function of the increasing vertical distance. A typical penetration depth (decay constant) is around 200 nm, which makes SPR very sensitive to the dielectric constant of individual nanoparticles at the interface.

It has been shown that LSPR can be easily excited by the incident light in DFM as long as its wavelength matches the plasmonic band of the nanostructures. However, SPPs can only be excited by using p-polarized light under particularly-designed optical configurations because SPPs place additional requirements on the matching of momentum in addition to energy. The Kretschmann configuration (dielectric/metal/dielectric structure) is one of the most commonly adopted optical systems in SPRM, as shown in Fig. 4a. The SPRM is built on an inverted microscope with total-internal reflection illumination in order to achieve light parallel to the metal–dielectric interface.[6,104,105] When the incident angle, thickness of the gold film and refractive index of the surrounding medium match each other, SPPs are generated and they propagate along the interface before entering the camera through the same objective due to total-internal reflection. There are three major differences in the optical configuration when comparing SPRM with TIRFM. First, a gold-coated coverslip is used instead of a glass coverslip. This is the core element for generating SPPs. Second, reflected light with the same wavelength as the incident light is collected by the camera, leading to the absence of optical filters or dichromic mirror. Third, p-polarized light is required to excite the SPPs. As the SPPs penetrate into the solution by ~200 nm, the presence of nanoparticles on the gold film disturbs the SPPs and alters the distribution of the local reflectivity in the SPRM image. In addition to the objective-based SPRM, a prism-based Kretschmann configuration is also capable of imaging single nano-objects with a compromised spatial resolution due to the optical distortion effect associated with the prism.[106–110]

Because the image contrast of a single nanoparticle is dependent on its dielectric constant, a physical property that applies to any material, SPRM is thus suitable for studying all kinds of

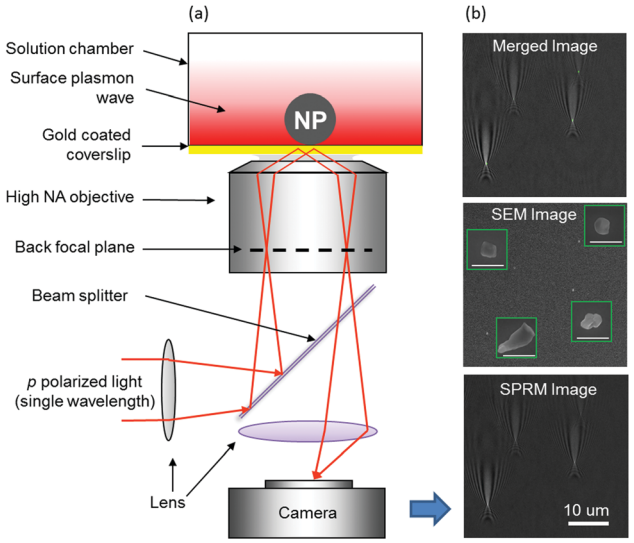

Fig. 4 (a) Representative optical configuration of an objective-based SPRM. (b) Each individual nanoparticle shows an identical PSF in the SPRM image, regardless of its size and morphology. Scale bars in the four inset SEM images: 400 nm. (b is reprinted with permission from ref. 114. Copyright 2017, American Chemical Society.)

nanomaterials, including metal,[108,111,112] semiconductor,[17,105,113] metal oxide,[114] and organic polymer nanoparticles,[115–117] as well as biological nanoparticles, such as bacteria,[118–120] vesicles[121,122] and viruses.[6,123] SPRM intensity scales down at the third order of decreasing diameter.[105,112] Therefore, it is more sensitive for detecting small nanoparticles than DFM, whose signal scales down at the sixth order of size. For example, individual 20 nm gold nanoparticles can be routinely imaged by SPRM with good SBR.[105,124] More importantly, SPRM allows for the visualization of soft nanomaterials, such as viruses,[6] protein nanoparticles[123] and nanobubbles,[17] without the need for labeling.

SPRM exhibits a quite special PSF. The bottom panel in Fig. 4b shows an SPRM image of four $LiCoO_2$ nanoplates whose scanning electron microscopy images are displayed in the middle panel. The excellent co-localization shown in the merged image (top panel) demonstrates that a single nanoparticle produces a wave-like pattern with parabolic tails regardless of its size and morphology. Existing studies have confirmed that a similar pattern was also observed for various types of nanomaterials with different chemical compositions.[6,17,105,111,112,114,115,123,125] Therefore, it can be concluded that such a wave-like pattern represents the PSF of SPRM. Both theoretical[121,126,127] and experimental[128–130] investigations suggested that the as-obtained PSF is due to the interference between the reflected incident light and the scattered surface plasmon polaritons by the nano-objects.

Mechanisms for applications rely on the sensitive dependence of SPRM intensity on the dielectric constant and size of the nanoparticle, as well as the vertical distance between the nanoparticle and the gold film. This principle is somewhat similar to the antenna mechanism which is adopted in DFM for studying hybrid plasmonic–dielectric nanomaterials. The gold film and the corresponding SPPs act as an antenna to detect

chemical events that alter the dielectric constant of the nanoparticles. Molecular interactions occurring on the nanoparticle,[116,120] volume shrinkage of the nanoparticle,[112] and altered chemical composition of the nanoparticle due to substance uptake[125] and reactions[113,114] have all been demonstrated to affect its optical signal. The refractive index of the surrounding medium also matters. Photocatalyzed[17] and electro-catalyzed[111] hydrogen evolution reactions generated H_2 molecules, leading to a decreased local dielectric constant. The correspondingly reduced optical signal thus allows for interrogation of the catalytic activity of single CdS and Pt nanoparticles, respectively. Thermal dissipation of a single gold nanorod after heating by an excitation beam reduced the refractive index of the local solvent, which was used to quantify its photo-thermal efficiency.[131] In addition to the dielectric constant, the SPRM intensity of the nanoparticle is also affected by the nanoparticle–substrate distance due to the near-field feature of SPPs. An oscillator strategy was proposed to determine the surface charge of single nanoparticles by measuring the vertical movement of a charged nanoparticle under a modulated driving electric field.[132,133]

The gold film in the SPRM naturally facilitates its applications in electrochemistry by playing two roles simultaneously. It not only acts as the optical interface to excite SPPs, but also as the electrode to trigger electrochemical reactions. The overlapping of diffusion layer ($\sim$microns) and penetration depth of SPPs (sub-microns) make SPRM a sensitive detection technique by taking full advantage of the near-field feature of SPPs and the near-surface feature of electrochemistry. The SPRM signal is also affected by internal (electron density in gold film) and external factors (the nanoparticle itself, surface adsorbates and the surrounding medium). Such dependence allows SPRM to detect both Faradaic electrochemical reactions[134] and non-Faradaic charging current.[135] In a Faradaic reaction, reactants in the bulk solution receive electrons (or lose electrons) to be reduced (or oxidized) to product molecules, leading to a different refractive index of the local solution or the nanoparticle itself.[136] In a non-Faradaic charging process, increased or decreased electron density alters the dielectric constant of the gold film.[137] By applying appropriate optical-to-electrochemical conversion models, one can achieve high-resolution electrochemical imaging without the need for recording current.[134,135]

Raman microscopy

A Raman microscope measures the inelastic scattering spectrum of monochromatic illumination by substances due to their vibrational and rotational modes. The Raman signal is usually several orders of magnitude lower than that of Rayleigh scattering due to the extremely small Raman scattering cross-section. As a result, direct measurements of the spontaneous Raman spectrum of individual objects have been only possible for micron-sized objects, such as inorganic microspheres[138] and biological samples.[139] However, the presence of nanoscale hot spots is able to dramatically enhance the Raman signal by 6–10 orders of magnitude due to both electromagnetic and chemical enhancement mechanisms, allowing for the imaging of single nanoparticles and even single molecules.[4,140–144]

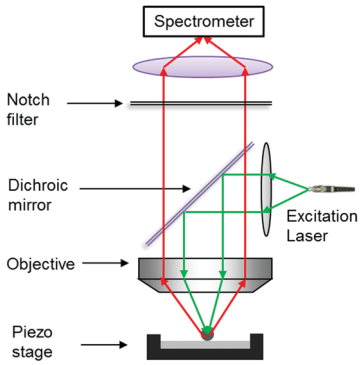

Fig. 5 Representative optical configuration of an upright Raman microscope.

Fig. 5 illustrates an upright laser-scanning confocal configuration that is often adopted in Raman microscopes as it is more compatible with a non-transparent substrate. The excitation beam is collimated and focused at the sample *via* a confocal design because it provides sufficient excitation density to improve the SBR. Inelastic scattering photons are collected with the same objective, which subsequently go through a dichroic mirror and notch filter to remove the elastic scattering background. A spectrometer is utilized to obtain the Raman spectrum of this particular point in the sample plane. *X*–*Y* scanning of the sample stage or the excitation beam thus delivers a Raman image containing spectroscopic information about each location (pixel).

Three of the most important features of surface enhanced Raman spectroscopy (SERS) imaging are hot spots, single molecule sensitivity and chemical identity. Hot spots are nanoscale regions with sharp geometries (such as edges, curvatures, gaps and junctions) that exhibit dramatically enhanced local electromagnetic fields. They play essential roles in enabling the SERS detection of single molecules because the Raman signal scales as the fourth power of the magnitude of the local electromagnetic field.[145] The existence and distribution of hot spots in a surface can be indirectly visualized by mapping the localization of single-molecule SERS bursts,[12,146] which are further correlated with the geometrical structure.[147] For example, the deposition of a metal film on a closely-packed monolayer of nano-spheres resulted in periodic hot spots that are spatially correlated with the inter-particle gaps.[148] A core–shell structure is also introduced to probe the Raman spectrum of the shell nanomaterials or the substrate by taking the plasmonic core as the nano-antenna.[149] Although plasmonic nanostructures are deeply involved in both DFM and SERS, there is a major difference between them. While an isolated spherical metal nanoparticle itself is able to produce sufficient SBR in DFM, plasmonic coupling between two plasmonic elements is often required to create hot spots for SERS imaging. These include inter-particle gaps in dimer and oligomer aggregates of plasmonic nanoparticles, edges and curvatures within a single nanoparticle, nanogaps between a plasmonic nanoparticle or near-field tip and substrate. Because the sizes of these hot spots are compatible with those of molecules, SERS is particularly suitable for boosting the Raman signals of single molecules that are either surface-bound or freely diffusing into and out of these

hot spots.[150] Elaborate efforts have also been made to place nanomaterials such as single-walled carbon nanotube inside the nanogap,[151] so that the chemical processes occurring on these nanomaterials can be studied.[152] An alternative method is to deposit a thin-layer of non-plasmonic nanomaterials between a plasmonic nanoparticle and a metallic mirror.[153]

The single molecule sensitivity of SERS was first demonstrated on isolated silver nanorods[4] and aggregates of silver nanoparticles.[140] Because SERS is able to provide the chemical identity of individual molecules, it is most powerful for interrogating single-molecule reactions by monitoring the disappearance of characteristic Raman peaks in reactants as well as the appearance of new peaks associated with products.[30] However, altered vibration modes are often observed in single-molecule SERS experiments when compared with bulk measurements. Possible mechanisms include the preferred molecular orientation in confined spaces[154] and the altered electromagnetic field, as well as charge transfer processes.[155] For example, an intense electromagnetic field in a plasmonic nanogap was found to break the selection rule, leading to the appearance of a Raman peak that was associated with a theoretically forbidden electronic transition.[151] Although obvious spectral and intensity intermittency was also observed for SERS signals from single molecules,[156–161] they follow quite different mechanisms from FL photoblinking. Because the SERS spectrum and intensity are extremely sensitive to the local electromagnetic and chemical environments, thermal diffusion and rotation would cause stochastic changes in the localization, orientation and reactivity of a single molecule when it is in close vicinity to a hot spot.

Photothermal microscopy (PTM)

When a substance in an excited state returns to the ground state, it releases the absorbed energy through either non-radiative thermal relaxation (dissipation of heat) or radiative relaxation (emission of photons). For broad types of nanomaterials, thermal relaxation is the dominant pathway, leading to an increased local temperature *via* heat dissipation from the nanoparticle to the surrounding medium. PTM is one kind of optical microscopy that maps the photo-thermal efficiency of single nanoparticles by measuring the local temperature with optical approaches.[5,162] Compared with FLM and DFM that require the object to be fluorescent and plasmonic, respectively, PTM has greatly expanded the applicability for imaging broader types of light-absorbing nanomaterials, such as semiconductor nanocrystals[163,164] and carbon nanotubes,[165–167] in addition to plasmonic nanoparticles.[5,168,169] The improved SBR has further enabled the imaging of single organic chromophores at room temperature.[170]

Fig. 6a illustrates the representative optical configuration of PTM. Two beams, a heating beam and a probe beam, are often used in a PTM apparatus. The wavelength of the heating beam is located at the maximal absorption band to efficiently excite the nanoparticle and to increase the local temperature. The probe beam, however, is usually off the absorption band in order to detect the tiny temperature increase optically without disturbing the nano-object. It is the local refractive index that

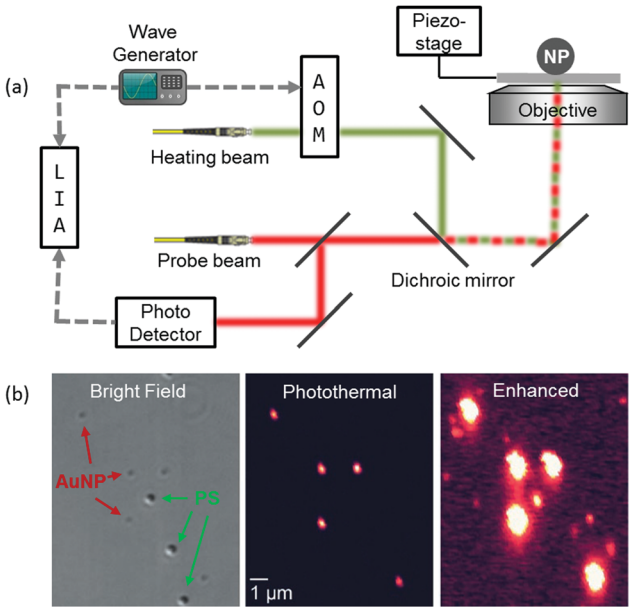

Fig. 6 (a) Representative optical configuration of a PTM. LIA: lock-in amplifier; AOM: acousto-optic modulator. (b) Bright field, photothermal and enhanced photothermal images of 300 nm polystyrene latex (green arrows), 80 nm gold nanoparticles (red arrows) and 10 nm gold nanoparticles (small dots in the enhanced image) ((b) is reprinted with permission from ref. 5. Copyright 2002, AAAS.)

connects the photothermal process and the optical readout, because a decreased refractive index always accompanies thermal dissipation. High-frequency modulation and optical interference are two essential components for achieving a sufficient SBR.[162] In a typical PTM, the heating beam intensity is modulated at a rather high frequency (*i.e.*, 1 MHz), resulting in a modulated local refractive index profile. As a result, the signal of the probe beam is accordingly modulated at the same frequency, which is detected with a lock-in amplifier. Note that one should not confuse PTM with the other photothermal imaging techniques that map the temperature distribution of macroscopic living samples (such as tissues and animals) by directly measuring the infrared radiation with an infrared camera. PTM does not map the distribution of temperature. Instead, it maps the distribution of photo-thermal conversion efficiency.

A representative PTM image of a mixture of gold nanoparticles and polystyrene nanoparticles is shown in Fig. 6b. The bright field image (left panel, differential interference contrast mode) confirms the existence of both 300 nm polystyrene (green arrows) and 80 nm gold (red arrows) nanoparticles. When the surface was heated with a modulated 532 nm laser beam, optical intensity fluctuations were only detected at the locations of gold nanoparticles, due to the effective photo-thermal conversion (middle panel). When the heating beam intensity was increased, 10 nm gold nanoparticles with a much smaller absorption cross-section were also detected (right panel). Polystyrene nanoparticles remain invisible in the enhanced PTM images, demonstrating the excellent capability of PTM to distinguish nano-objects based on their absorption cross-sections rather than their sizes (Table 1).

Table 1 Comparisons between the five types of optical imaging techniques

	TIRFM	DFM	Raman	SPRM	PTM
Principle	Fluorescence & evanescent wave	Rayleigh scattering & localized SPR effect	Raman scattering & localized SPR effect	Planar SPR effect & surface plasmon polaritons	Absorption of light & photothermal effect
Mechanisms for applications	(1) Intensity (enhancement, quenching) (2) Spectrum (anisotropy, lifetime, FRET) (3) Super-localization	(1) Spectral shift (as a result of chemical event) (2) Plasmonic ruler (3) Nano-antenna	(1) Spectrum (as a result of chemical event) (2) SERS & TERS	(1) Image contrast (as a function of size, dielectric constant and vertical distance) (2) Gold film as working electrode	(1) Photothermal conversion efficiency
Most important features	(1) Intermittency (FL photoblinking) (2) Sufficient S/B for single-molecule imaging	(1) Colorful (2) Rayleigh scattering spectrum of single NPs	(1) Chemical identity (2) Hot spots (3) Single molecule reactions	(1) Suitable for all kinds of nanomaterials (2) Very special PSF (3) Gold-coated coverslip	(1) Absorption spectrum of single nanoparticles (2) Single molecule sensitivity
Applicability	Fluorescent nanomaterials (QDs, polymer, metal clusters, up-conversion)	Plasmonic nanomaterials (gold, silver and hybrid nanomaterials)	Plasmonic nanomaterials (gold, silver and hybrid nanomaterials)	All kinds of nanomaterials (metal, oxide, semiconductor, polymer, soft nanomaterials)	Light-absorbing nanomaterials (plasmonic, carbon, semiconductor)
Light source	Single wavelength	White light	Single wavelength	Single wavelength	Single wavelength
Detector	Monochromatic camera	Spectrometer + camera	Spectrometer + camera	Monochromatic camera	Single-point photodetector
Major application fields	Nanoprobes for imaging, sensing and tracking; nanocatalysis	Nanoprobes for imaging, sensing and tracking; nanocatalysis	Single-molecule chemistry	Nanoelectrochemistry; nanocatalysis	Nanoprobes for imaging, sensing and tracking

Other optical imaging techniques

A couple of monochromatic interference microscopes, differential interference contrast (DIC) microscope and interferometric scattering microscopy (iSCAT), have also been developed to image individual plasmonic and dielectric nanomaterials, respectively. DIC is a classical optical microscope that is able to enhance the contrast of tiny objects by introducing interference between two mutually orthogonally polarized beams. Two Nomarski prisms are included in the optical path to separate and combine these two beams before and after they interact with the sample, respectively. As the incident beam is polarized, the relative orientation between the beam and an anisotropic nanorod influences its optical pattern in the image plane. Based on this dependence, Fang's group developed a single particle orientation and rotational tracking (SPORT) technique to interrogate the rotational diffusion of single anisotropic plasmonic nanorods.[171,172] The introduction of a series of band-pass filters reveals the wavelength-dependent DIC contrast of single plasmonic nanoparticles,[173] allowing for the study of the plasmon resonance energy transfer between nanoparticles and their surface adsorbates.[174]

In contrast to many techniques that are dedicated to reducing the background, iSCAT creates a stable background by introducing the interference between two coherent light beams that are separated with a 50/50 beam splitter. The utilization of a high-frequency acousto-optic deflector enables rapid and periodical beam scanning over a surface within one camera exposure time, leading to a pseudo wide-field image that is free of interference fringes and is capable of lock-in filtering.[175] Any change in the dielectric environment on the substrate caused by nanoparticle adsorption would be detected by subtracting the temporal background, which is the image just before the nanoparticle adsorption. A state-of-the-art iSCAT setup has demonstrated its capability of detecting and tracking single virus particles,[176] single quantum dots in the dark-state[177] as well as single protein molecules[178–181] without the need for FL labeling or plasmonic enhancement.

Nanosensing

Owing to their rich optical, magnetic, electrical and chemical properties, versatile nanomaterials have attracted intensive attention for the development of chemical and bio-sensors. When continuously capturing the optical images of single nanoparticles upon binding of analytes, each nanoparticle acts as a nano-sensor to report the molecular recognitions and interactions occurring on its surface. These nanosensors possess several unique advantages over bulk sensors composed of ensemble nanomaterials. First, the spectral linewidth of single nanoparticles is systematically narrower than that of the ensemble,[182] leading to improved sensitivity because it is easier to quantify the shift of a spectrum with a narrower linewidth. Second, because each nanosensor reports the qualitative and quantitative information about the analytes in an extremely confined local region, they are suitable for acting as nanoprobes to report the spatial distribution of chemical species[87] and physical properties[183] in microscopic and heterogeneous samples such as living cells.[184–188] On the other hand, each nanosensor exhibits significantly varying sensitivity and specificity due to their structural heterogeneity. Optical imaging

represents a high-throughput approach for exploring the structural dependence of analytical performances, with implications for the rational design and optimization of nanomaterials in bulk sensors.[189,190]

Mechanisms for signal transduction

Among several mechanisms for converting molecular binding events to detectable optical signals, the spectral shift of a single plasmonic nanosensor under DFM or PTM is one of the most powerful approaches.[71,188,191–193] Because the plasmonic band is sensitive to the dielectric constant of the surrounding medium (particularly that of surface adsorbates), the adsorption of analytes onto the nanoparticle surface,[3,194] or even a conformational change in the surface-bound molecules,[195] could change its optical property. In order to improve the selectivity, the nanoparticle was often functionalized with designed recognition molecules to enable specific interactions.[196] When the absorption spectrum of surface-bound molecules matched the scattering spectrum of the plasmonic nanosensor, quenching dips appeared in the observed scattering spectrum due to plasmon resonance electron transfer.[197] Signal-off[198] and signal-on[199,200] types of sensing mechanisms have been proposed by regulating the quenching efficiency between surface molecules and the plasmonic core. Similarly, the near-infrared fluorescence of single-walled carbon nanotubes has also been employed to develop single nanoparticle optical sensors.[44] Analyte binding altered the electronic structure of the nanotubes and led to a shift in the FL emission band or intensity change.[187] In addition to surface-bound molecules, auto-correlation analysis on the temporal fluctuation of the scattering intensity was used to determine the diffusion coefficient of the analytes even though they did not bind to the nanosensor, as they interfered with the plasmonic band when they simply diffused across it.[97]

An antenna strategy has become a popular way of studying hybrid nanomaterials consisting of plasmonic and non-plasmonic components by separating molecular recognition and signal transduction. The non-plasmonic component enables the molecular recognition of chemical reactions to induce a change in dielectric constant. The presence of an adjacent plasmonic component subsequently converts such a change to a spectral shift. For instance, hydrogen adsorption reduces the dielectric constant of a nano-sized Pd disk, leading to a red-shift of the scattering spectrum of an adjacent triangle-shaped gold nanoparticle.[201]

In order to further amplify the spectral shift upon analyte binding, a couple of strategies have been developed: etching/precipitation[78,85,202,203] and a plasmonic ruler.[204,205] In the former case, the presence of analytes induces a morphological and compositional change in the plasmonic sensor, which is often accompanied by a rather large spectral shift up to 100 nm.[202] For example, it was proposed that the self-catalytic growth of a plasmonic nanoparticle would amplify the spectral shift as the scattering intensity increased by the sixth power of its size.[206] In the latter case, the plasmonic coupling effect between a pair of metallic nanoparticles is extremely sensitive to the inter-particle distance, allowing for the reporting of a sub-nanometer

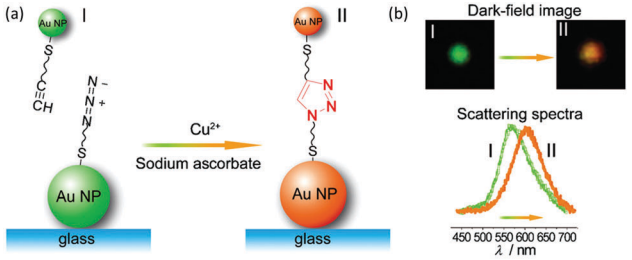

Fig. 7 (a) Two kinds of Au nanoparticles are functionalized with azide and alkyne groups, respectively. The presence of Cu(I) triggers the click-chemistry reactions and conjugates these nanoparticles. (b) The reaction process results in a color change from green to orange under DFM, which is accompanied by a shift in the plasmonic band (reprinted with permission from ref. 207. Copyright 2013, WILEY-VCH Verlag GmbH & Co. KGaA, Weinheim).

change in the inter-particle distance induced by biomolecule interactions[204] or click-chemistry reactions.[207] Click chemistry refers to a powerful Cu(I)-catalyzed cycloaddition reaction that conjugates an azide group and an alkyne group to form a 5-membered heteroatom ring. Long and co-workers functionalized 60 nm and 14 nm Au nanoparticles with azide and alkyne groups, respectively (Fig. 7a). The presence of Cu(I) was found to trigger click-chemistry reactions and recruit 14 nm Au nanoparticles at the surface of pre-immobilized 60 nm Au nanoparticles, leading to an obvious color change from green to orange under DFM as well as a large red-shift in the plasmonic band (Fig. 7b).[207] Such a system allowed for the detection of copper ions with excellent selectivity and sensitivity. In contrast to many single-nanoparticle sensing studies that relied on non-covalent molecular recognition, this work suggested the advantage of covalent interactions in developing highly specific nanosensors. The combination of DNA nanotechnology with a plasmonic ruler is an interesting approach.[208,209] With the aid of precisely tailored DNA origami, the inter-particle distance can be designed and regulated in the presence of analytes.[208] A special form of plasmonic ruler modulates the vertical distance between a nanoparticle and a plasmonic substrate. When applying a periodically modulated driving potential to the substrate, charged nanoparticles accordingly oscillated along the vertical direction, which was accompanied by modulated optical intensity due to the periodic plasmonic coupling. It was proposed that such nano-oscillators could determine the surface charge of an individual nanoparticle,[133] which was further utilized to measure the phosphorylation kinetics of a surface-bound peptide in the presence of kinase.[132]

Towards single-molecule detection and imaging

Single-molecule detection has been achieved in many optical imaging techniques with different approaches.[8] In one scenario, optical signals from the single molecule itself are strong enough to be directly imaged with a sufficient SBR. These techniques include FLM, PTM and iSCAT. While single-molecule FL imaging has been well established and accepted, other techniques are still on their way towards routine applications. Sophisticated optimizations of the experimental conditions, including types of

media and chromophores, substrate as well as light source, are required in PTM.[170,210] SPRM and iSCAT are able to image biological molecules with rather large molecular weights.[178,211,212] In the other scenario, the detection of single molecules was achieved with the help of signal amplification elements such as hot spots. They include SERS, DFM and PTM. A hot spot exhibits extraordinary sensitivity to the attachment of a molecule in its center by enhancing the FL and Raman signal of the molecule. On the other hand, light–molecule interactions also influence the plasmonic scattering of the hot spot itself.[213] This tiny effect can be detected by measuring the spectral shift in DFM,[95] or by monitoring the change in extinction coefficient at a fixed wavelength with PTM.[214] In a recent study, this concept has been pushed to a single atomic ion interaction with a plasmonic nanorod *via* a whispering gallery mode sensor.[215]

Nanoelectrochemistry

Versatile types of nanomaterials have been widely used in broad electrochemistry fields, including batteries and fuel cells, electrocatalysis, electro-deposition and electrochemical sensing. In order to evaluate the electrochemical activity of single nanoparticles, one has to determine the electron transfer rate occurring at single nanoparticles as a function of electrode potential or time. Despite the great efforts towards single-nanoparticle electrochemistry,[178,216,217] this task remains quite challenging because the conventional recording of an electrode current lacks spatial resolution. As an alternative and complementary approach, optical microscopy has been emerging rapidly in the past decade to study the electrochemical activity of single nanoparticles. Instead of measuring the electrode current electrically, optical microscopy determines the local electron transfer rate through pure optical signals.[216] FLM,[217–219] DFM[79,220] and SPRM[134–136,221] are among the earliest microscopes for acquiring local electrochemical information optically. To satisfy both optical and electrochemical requirements, transparent conducting substrates such as indium tin oxide (ITO) and fluorine-doped tin oxide are often needed for inverted microscopes, such as FLM, DFM and PTM. For SPRM and SERS, a gold-coated coverslip is naturally applicable. Other options include a semi-transparent copper grid (for transmission electron microscopy characterizations) and glass modified with a thin layer of conducting polymer or graphene.

Optical voltammetry of single nanoparticles

Voltammetry is a powerful electrochemical technique to determine reaction kinetics and mechanisms by measuring the electron transfer rate as a function of potential. Several studies have demonstrated how optical microscopy can resolve the optical voltammetry of single nanoparticles in direct electrochemistry. As shown in Fig. 8, it was found that the extraction of Li^+ ions from $LiCoO_2$ nanoparticles generated a de-lithiated oxidation product, $Li_{1-x}CoO_2$, which exhibited a linearly decreasing dielectric constant with a decreasing amount of lithium, accompanied by decreasing optical intensity in SPRM (Fig. 8a).[114]

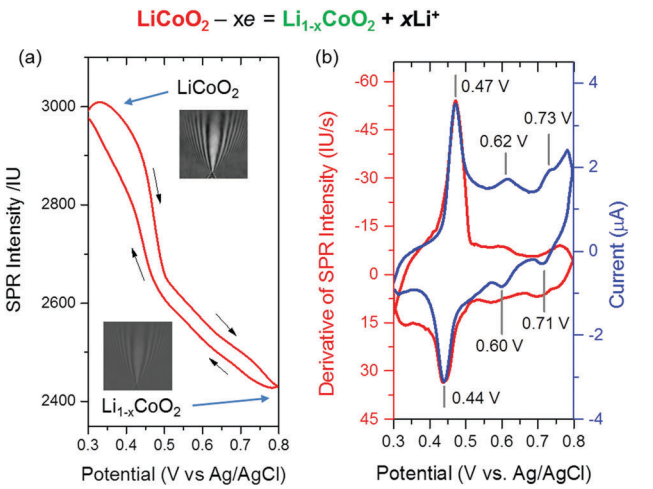

Fig. 8 (a) Electrochemical de-lithiation and lithiation of a single $LiCoO_2$ nanoparticle is accompanied by a decrease and recovery in its optical intensity. (b) The time derivative of the optical curve allows for determination of the cyclic voltammogram of single $LiCoO_2$ nanoparticles, which is well consistent with the conventional cyclic voltammogram obtained from bulk measurement (reprinted with permission from ref. 114. Copyright 2017, American Chemical Society).

As a result, the time derivative of the SPRM curve provided the insertion or extraction rate of Li^+ ions, which was equivalent to the electron transfer rate (Fig. 8b). Therefore, the optical voltammetry of single nanoparticles can be calculated from time-lapsed SPRM images. Such an optical-to-electrochemical conversion model was experimentally validated in a subsequent study by simultaneously recording the optical and electrochemical signals during the collision of single $LiCoO_2$ nanoparticles.[222] Similarly, the optical voltammetry of a single gold nanowire was also determined by calculating the time derivative of its optical signals during redox cycling, owing to the different dielectric constants between oxidized and reduced gold nanowire.[223] Prussian blue is a well-known type of electrochromic material whose absorption property (the imaginary part of the refractive index) can be modulated *via* electrochemical reactions. Accordingly, the optical voltammetry of a single Prussian blue nanoparticle was resolved from the time derivative of optical signals during cycling.[224] This conversion model is also applicable for obtaining the optical voltammetry of single nano-sized droplets containing the electroactive dye, Nile Red, under FLM.[225] The reduction of fluorescent Nile Red molecules formed a non-fluorescent product, leading to decreased fluorescent intensity, which was recovered in the oxidation process.

In addition to the dielectric constant, the dependence of optical intensity on the size of nanoparticles has also been introduced to monitor the deposition and dissolution processes of metal nanoparticles. Pan *et al.* monitored the growth process of individual silver nanoparticles with DFM when triggering electro-deposition under a sweeping potential.[75] Significantly increased scattering signals were recorded as a result of the increasing size of the silver nanoparticles. By establishing a calibration curve between the scattering intensity (under monochromatic illumination) and size, they were able to calculate the

reaction current of single nanoparticles. Spectral evolution offered additional information regarding the growth and reaction mechanism of metal nanoparticles, as demonstrated by Long and coworkers.[76] Three important parameters, the wavelength with maximal scattering, scattering intensity and spectral line width, were extracted from time-dependent single-nanoparticle spectra. Monitoring the electrochemical deposition and stripping of mercury onto single gold nanorods revealed critical steps in the amalgamation.[226] Combined FLM and DFM have been employed to study the same potential-dependent deposition and dissolution processes of silver nanoparticles by monitoring the photoluminescence and plasmonic scattering signals, respectively.[227] The reverse processes, *i.e.*, the oxidative dissolution of pre-immobilized silver and copper nanoparticles, have also been investigated because the formation of dissoluble cations reduced the size of the nanoparticles, leading to decreasing optical signals.[108,112] The results have shown that the oxidation potentials of single nanoparticles are largely dependent on the chemical composition and surface ligands. Single-nanoparticle studies also revealed that a population of nanoparticles underwent incomplete dissolution due to the formation of the passivated metal-oxide layer, which was evident from the residual optical signals after reactions.[228]

The electrochemical activity of freely diffusing nanoparticles can also be studied by simultaneously monitoring the optical images and electrochemical currents when they stochastically collide on the electrode surface.[184] In a typical single-nanoparticle collision study, an appropriate potential was applied to an inert ultramicroelectrode to achieve a relatively low background current. The collision of electroactive nanoparticles onto the electrode triggered transient and local electron transfers, leading to a current spike that reflected the electrochemical activity of the individual nanoparticle. The combination of optical microscopy and single-nanoparticle collision helps clarify several technical concerns. First, optical microscopy provides direct evidence confirming that the current spike is indeed due to the collision of a single nanoparticle, by watching the collision events optically. This is important because it could be difficult to determine whether a large (or wide) current spike is due to a single nanoparticle with outstanding activity, or the simultaneous collision of multiple nanoparticles.[112] Second, optical imaging reveals additional information regarding the moment and location of a collision, as well as the subsequent vibration and migration of nanoparticles.[229] For example, Kanoufi *et al.* reported that the current spike sometimes appeared a few milliseconds before a single Ag nanoparticle began to shrink in size, suggesting that the electron transfer and the formation of dissoluble silver ions were not completely synchronized processes.[230] More importantly, the collision strategy validates the optical-to-electrochemical conversion model by quantitatively comparing the optical and electrochemical currents.[222,231]

The conversion model is more complicated in electrocatalysis when considering the rapid diffusion of both reactant and product molecules. In a milestone study, Tao and co-workers established a quantitative model by taking the species diffusion into consideration, leading to a semi-derivative relationship between the optical signal (the local concentration of reactant/products) and the electrode current.[136] This relationship was utilized to calculate the hydrogen generation rate of a single Pt nanoparticle during the electrocatalyzed hydrogen evolution reactions.[111] Species diffusion not only complicated the optical-to-electrochemical conversion model, it also greatly reduced the effective optical signals, due to the decreased local concentration. Therefore, indirect approaches were proposed to facilitate electrocatalysis studies by focusing on electro-active species that were bound on the nanoparticles[232] or by forming a new phase at the nanocatalyst surface, such as a gas bubble[233] or deposition.[234] The electrochemiluminescence reaction of a ruthenium complex[235–237] catalyzed by gold nanoparticles was also suggested for imaging electrocatalysis without the need for a light source. Spontaneous light emission from ECL reactions surrounding a gold nanowire suggested its catalytic activity. A surface layer of gel was required to minimize the diffusion of emitting products in order to improve the SBR.[235] In a recent study, Xu and Chen designed an asymmetrical Au–Pt Janus structure to reduce the oxidation and poisoning of a metal nanoparticle by introducing local turbulence as a result of the different reaction rates at the Au and Pt components, leading to significantly enhanced stability and SBR in the ECL imaging of single nanoparticles.[237]

Non-Faradaic charging

The dependence of nanomaterials' optical properties on their density of states has been utilized to study the non-Faradaic charging process, with implications for developing supercapacitor devices. For plasmonic nanoparticles, the extinction band relies on the frequency of the resonant oscillation of free electrons, which depends strongly on the number density of electrons in a nanoparticle. Mulvaney *et al.* reported the reversible spectral shift of a single gold nanorod when it underwent electrochemical charging and discharging.[79] A cathodic potential of −1.4 V was found to induce a blue shift in the longitudinal scattering band by 11 nm, which was attributed to the injection of 85 000 electrons, according to an estimation based on the free electron model of metals and the discrete dipole approximation method. The size and morphology did not change before or after the electrochemical process. In addition to the direct non-Faradaic charging, the literature has suggested other methods for charging plasmonic nanoparticles, including chemical reactions at the nanoparticle surface[81,82] and electrochemical reactions of co-existing electroactive species.[238] In order to push the sensitivity towards quantized electron transfer, an ion gel capacitor with enhanced double-layer capacitance was introduced into a solid-state device to further improve the charge density, as shown in Fig. 9.[80] Furthermore, intensity detection at an optimized single wavelength was proposed to replace the spectral fitting, leading to improved temporal resolution and sensitivity. A capability of detecting the injection of fewer than 110 electrons into a single gold nanorod was achieved in their recent work.[80]

The comprehensive mechanism remains to be clarified when interpreting the spectral shift during electrochemical charging,

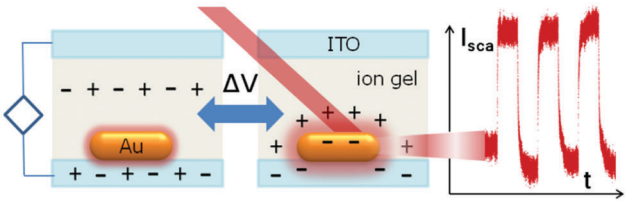

Fig. 9 Non-Faradaic charging and discharging of a single gold nanorod resulted in reversible changes in its scattering intensity. The presence of an ion gel capacitor is able to dramatically enhance the signal (reprinted with permission from ref. 80. Copyright 2016, American Chemical Society).

because the plasmonic feature is not only influenced by the electron density but also by the surrounding dielectric environments, such as rearrangement of adsorbates and counter ions. These processes are often reversibly concomitant with the electrochemical charging and discharging cycles. The weak adsorption of anion species to the gold nanorods,[239,240] as well as the dynamic formation of metal-halide[241,242] and metal-oxide complexes,[223,242] was found to affect the plasmonic feature. The dynamic concentration gradient of counter ions in the diffusion layer also influenced the optical signal. Statistical analysis of hundreds of individual nanoparticles revealed the co-existence of multiple populations obeying different electrochemical tuning mechanisms.[243] The optical response of a gold nanorod can also be electrically modulated by coating the nanorod with a thin-shell of non-linear optical material.[244] Polarization of the dielectric constant distribution in the shell under an external electrical field was able to rapidly and reversibly modulate the plasmonic band of the gold nanorod.

Tao's group took different approaches to determining the non-Faradaic charging of metal nanowires[245] and 2-dimensional graphene.[246,247] Electrochemical charging and the concomitant anion adsorption reduced the surface stress of a gold nanowire, leading to elongation along the axis. An optical edge tracking method was developed to determine the tiny elongation, from which the surface stress of the nanowire could be accessed.[245] It was further found that, when charging 2-dimensional graphene, Pauli repulsion resulted in the edge expansion of a graphene monolayer that was loosely attached at the substrate. A similar edge tracking method allowed for determination of the mechanical properties of the nanomaterials.[247]

Strengths and remaining challenges

The optical read-out of single-nanoparticle electrochemistry shows a couple of promising strengths to improve the sensitivity and throughput compared with conventional electrochemical recordings. Optical voltammograms were able to detect current peak down to sub-pA without the need for suppressing the background current with an ultramicroelectrode.[114] Owing to the ultimate sensitivity of single-molecule detection, single-molecule electrochemical reactions have been investigated by monitoring the FL burst due to the production of a single fluorescent product molecule[248–251] or the appearance of a characteristic SERS vibrational mode.[232,252,253] As a matter of fact, optical microscopy has been one of the major options for studying single-molecule electrochemistry.[29,254] In addition, the spatial resolution of optical microscopy renders high throughput to measure the electrochemical activity of tens to hundreds of individual nanoparticles in a single measurement. The very same individuals can be re-visited with other high-resolution structural characterization techniques, such as electron microscopy, offering an efficient way to bridge the structure and activity at single-nanoparticle level.[114,222,227]

Existing studies have also raised important questions and challenges. While the optical readout of direct electrochemistry has been well developed, it is more difficult to determine the electrocatalytic activity of a single nanocatalyst, due to its smaller size and the diffusion of reaction species. The introduction of a confined space has proven to be an effective way to slow down the diffusion.[235,250] An alternative option is to improve the temporal resolution of optical recording so that the diffusion length can be greatly reduced within a shorter exposure time. Moreover, the requirement for the transparency of the electrode for optical imaging excluded the majority of common electrode materials. The deposition of a thin layer of ITO or metal onto quartz glass is known to produce a rough and heterogeneous surface, making it difficult to form a nanoparticle–electrode junction with good and controllable electrical contacts. Such variability might introduce additional heterogeneity.

Nanocatalysis

Catalytic activity is probably one of the most attractive properties of nanomaterials. Numerous studies have demonstrated the varied catalytic activity between and within individual nanoparticles, thus driving the development of single nanoparticle catalysis over past decades.[255] Very soon after the breakthrough of single-entity FL imaging,[1,2,13] Xie *et al.* studied the enzymatic dynamics of single cholesterol oxidase molecules by monitoring the fluctuating FL signal as a result of discrete enzymatic turnover events.[18] Emission was from the active center of this enzyme, which was naturally fluorescent in its oxidized form. The formation of a non-fluorescent intermediate reduced the FL intensity, so that the enzymatic kinetics was resolved by analyzing the FL intensity trajectory. Heterogeneous catalysis of organic reactions at a micron-sized layered double hydroxide crystal was then investigated with FLM by Hofkens and co-workers.[10] Facet-dependent catalysis was directly visualized by watching the spatial distribution of fluorescent products. The catalytic activity of single metal nanoparticles was subsequently achieved on FLM[19] and DFM.[81] Since then, many different techniques and methodologies have been proposed, which are summarized below.

Single-molecule fluorogenic reactions

The single-molecule fluorogenic reaction is the most widely adopted strategy to probe the catalytic activity of single nanoparticles. Since it has been well summarized in several reviews elsewhere,[255–259] here we focus on the basic concept and the most recent results. Individual nanocatalysts are immobilized

on the substrate in the presence of a reactant and a solvent. As the reactant molecules and nanocatalyst are not (or only weakly) fluorescent, a rather low background is observed under FLM. An optimized concentration of reactant is selected to allow for single-molecule turnover events in which a pre-adsorbed non-FL reactant molecule is converted to an FL product, leading to an FL burst at the location of the nanocatalyst. Desorption of products removes the FL signal and recovers the dark background for further reactions and observations. Counting the frequency of FL bursts around one nanocatalyst allows for quantitative evaluation of its catalytic activity.[19] Furthermore, when mapping the location of each FL burst with a super-localization algorithm, one can study the intra-particle distribution of catalytic activity at a spatial resolution of 40 nm.[260] Further improvement in the spatial resolution requires an enhanced SBR for each FL burst and the reduction of both optical and mechanical noise. In a recent approach, the projection of the super-localization of FL bursts onto a spherical hybrid nanocatalyst allowed for mapping of the 3-dimensional distribution of active sites on its surface.[261]

This strategy has proven successful for clarifying nanoscopic reaction kinetics and mechanisms,[262,263] for exploring structure-dependent activity,[264–269] and for revealing temporal fluctuation and spatial heterogeneity at single-nanoparticle and sub-nanoparticle levels.[259,270–272] For example, statistical analysis on the duration times of a series of alternating dark (t_{off}) and bright (t_{on}) states provided quantitative information on reaction kinetics and pathways. It has been postulated that the former (t_{off}) is relevant to the formation rate of products and the latter (t_{on}) represents its dissociation rate.[19] In a recent study, the activation energies of these two sequential steps were determined by measuring the characteristic times as a function of temperature.[262] Moreover, mapping the sub-nanoparticle distribution of catalytic activity revealed significant spatial heterogeneity. Further correlation with morphology provided a convenient way of clarifying the dependence of activity on several structural features, such as components,[273] facets,[265,274] defects,[260,269] hetero-junctions[270] and sizes.[267,275] Further, auto-correlation analysis of the FL trajectory reveals temporal fluctuation in the catalytic activity, which has frequently been observed in single-nanoparticle experiments at different time scales ranging from seconds to hours. Possible mechanisms include the spontaneous or reaction-induced re-arrangement of surface atoms[19,267] and intermittent interfacial electron transfer rates,[17,276] as well as the dynamic adsorption and desorption of surface adsorbates (poisoning).[271] Continuous recording revealed the gradual loss of catalytic activity of an individual Pd/C catalyst due to the electrochemical etching of small Pt nanoparticles.[272]

In addition to mechanistic studies, the structure–activity relationship revealed by single-molecule imaging is able to help in the rational design of nanocatalysts, which is more important for industrial catalysis. When mapping the location of active sites with single-molecule fluorogenic reactions in transition-metal-catalyzed polymerization[277] and copper-nanocrystal-catalyzed click chemistry,[278] one could identify the true catalytic active components, such as the surface of the nanoparticle or leaching molecule in solution, which is vital for differentiating between homogeneous and heterogeneous catalysis, with implications for helping in the design and application at bench scale.[279,280] Quantitative imaging and 3-dimensional localization of FL bursts allowed for an evaluation of the effect of steaming post-treatments on the catalytic activity of a single zeolite crystal.[281] Recently, Chen *et al.* found the unexpected co-localization of oxidative and reductive reaction centers and suggested that up-regulating the active sites with lower original activity tended to improve the overall catalytic activity more efficiently.[11]

While the fluorogenic reactions offer sufficient SBR to count and to locate single-molecule turnover events, they have several drawbacks. To date, only limited model reactions have been developed to study oxidation and reduction reactions, as summarized in a recent paper.[258] For those chemical reactions that do not involve FL-active compounds, FL tags can be introduced to light up the reaction,[277] although the labeling might alter the nature of the chemical reactions. For example, two FL moieties were linked to azide and alkyne molecules to act as donor and receptor, respectively. A click reaction catalyzed by single copper nanoparticles produced a conjugated structure, which was detected *via* the Forster resonance energy transfer mechanism.[278] More importantly, observations on the FL bursts require the product to stay at the nanocatalyst surface for a time period ranging from hundreds of milliseconds to tens of seconds, so that the photo-detector can accumulate sufficient photons for detection. Because the adsorption/desorption equilibrium is highly dependent on the physical and chemical property of the molecules, further studies are required to evaluate the possible bias caused by the selection of the fluorogenic model reaction. Fluorogenic reactions also affected the maximal turn-over rate of the nanocatalyst, as the simultaneous appearance of multiple bursts is not recommended in most studies. So far, an apparent turn-over rate as small as 0.01–0.1 s^{-1} has typically been reported in the existing literature. In addition, the FL intensity of single molecules is known to be influenced by photo-blinking and photo-bleaching, as well as by local enhancement and quenching mechanisms.[282] These effects are also spatially heterogeneous and fluctuate temporally.

Raman reporter molecules

SERS and TERS microscopy[283,284] have also been utilized to study nanocatalysis, owing to their chemical identification and single-molecule sensitivity. The basic concept is similar to that of fluorogenic reactions. Individual or a few molecules are adsorbed at a plasmonic hot spot, revealing the characteristic Raman spectrum of this reactant. Chemical reactions convert them to products, accompanied by the evolution of new peaks in the local Raman spectra. Because SERS has a unique advantage for chemical identification, analyzing the peak position and the peak intensity, as well as the spatial super-localization during the reaction, allows for the identification of the important intermediates and for the interrogation of the catalytic mechanism. However, the single-molecule sensitivity of SERS is extremely dependent on the plasmonic amplification, which

limits its applicability to broad types of non-plasmonic nanocatalysts. Unlike DFM, simple combinations of plasmonic elements with non-plasmonic nanocatalysts are usually not sufficient to produce hot spots for SERS imaging. Because of the technical difficulties of placing a nanocatalyst into a SERS hot spot,[151,152] current research focuses more on single-molecule chemistry.[30]

Spontaneous fluctuations in the spectrum and intensity of the single-molecule SERS signal is probably one of the most practical obstacles for studying single-molecule chemistry.[160] While chemometric algorithms have been proposed to separate valuable reaction kinetics from spontaneous fluctuations based on different time scales,[285] well-defined hot spots and stable metal–molecular–metal junctions are still preferred to reduce these fluctuations. A particular example was to place isolated metal nanoparticles over a flat metal film that was previously functionalized with reactant molecules.[286,287] Dimerization of 4-nitrobenzenethiols to form 4,4′-dimercaptoazobenzene was continuously monitored at single-molecule and single-nanoparticle level.[286] For each hot spot, the decreasing Raman peak intensity of the reactants was nicely consistent with the increasing signal of the products. However, significant heterogeneity was observed in the reaction rate and yield between different hot spots. A shift in the characteristic vibrational peak in the initial stage of the reaction identified the formation of an important radical intermediate.[288] In an earlier study, there was a reduction of the same compound in hot spots contributed by single gold nanoparticle dimers. This uncovered an intramolecular dissociation reaction pathway, as the inter-molecular distance was too large for classical dimerization.[289] A series of aromatic molecules are assembled in a molecular tunneling junction consisting of a gold nanoparticle and a flat gold mirror. The structure-dependent evolution of SERS spectra revealed the different transport mechanisms of hot electrons.[287] This work proposed an optical approach to study molecular electronics.

As the plasmonic nanostructures are also electrically conducting, it is suitable for studying electrocatalysis. Because the oxidized form of Nile Blue A produced a much larger resonant SERS signal than the reduced form, it acted as a reporter molecule to probe the redox activity of nanoparticles.[252] Super-localization of the Raman emission centroid revealed a periodical and reversible shift in the centroid trajectory during electrochemical cycles, suggesting site-specific redox potentials within the aggregates of silver nanoparticles.[232] Correlating the reactive sites with the aggregate morphology helped an understanding of the structural basis of such heterogeneity.[290] In order to take full advantage of the different vibrational bands, dual wavelength excitations were proposed to achieve the resonant SERS for reactant and product molecules.[291]

Owing to the chemical activity of plasmon-induced hot carriers,[289] the SERS approach inevitably superposed the plasmon-assisted catalysis of metallic nanostructures and their intrinsic catalysis. The presence of an enhanced electromagnetic field not only excites the Raman spectrum for characterization, but is also deeply involved in the optical, thermal and chemical aspects of chemical reactions.[287] Only those molecules adjacent to a plasmonic hot spot provided sufficient Raman signals for observation, blurring the difference between optical hot spots and chemically active sites. In addition, an intense laser is often required to effectively excite Raman scattering, and thermal dissipation increased the local temperature and accelerated the chemical reactions.[292]

Gas-generating reactions

Many important catalytic reactions do not involve substances with an FL property or plasmonic hot spots, such as hydrogen evolution reactions (HER) and oxygen evolution reactions (OER). Instead, these reactions naturally produce gases, which were utilized to quantify the catalytic activity without the need for artificial model reactions, according to several recent studies.[17,111,233,293] Gas-generating reactions are frequently encountered in many catalytic processes, such as water-splitting, electrolysis, nanomotors and artificial catalases. In order to avoid the rapid diffusion of hydrogen molecules, a sophisticated CdS@Au core–shell nanostructure was synthesized, in which hydrogen molecules generated by the photocatalysis of CdS shell accumulated inside the capsule and caused a red-shift in the plasmonic spectrum of the Au core.[293] Instead of introducing a capsule structure, the quantification of hydrogen generation can be much simplified by the formation of nano-sized gas bubbles in the catalytic decomposition of formic acid by Pt/Ag nanoparticles[233] and the photocatalytic reduction of water by CdS nanoparticles.[17] In the former case, the formation of hydrogen bubbles altered the plasmonic scattering of Pt/Ag nanoparticles under DFM (Fig. 10a). In the latter case, the hydrogen nanobubble reduced the refractive index of the local medium surrounding a CdS nanoparticle, which was detected by SPRM (Fig. 10b). An *in situ* FL labeling strategy was recently developed by the same group to light up the nanobubbles under common and conventional FL microscopes (Fig. 10c).[294] In this work, H_2 nanobubbles were generated at the surface of single CdS nanoparticles during photocatalysis. They recruited and accumulated hydrophobic FL molecules (rhodamine 6G) onto the liquid–air interface, leading to improved FL intensity under microscopes. The growth rate and the maximal SPRM or FL intensity were subsequently used to determine the photocatalytic activity of single CdS nanoparticles.

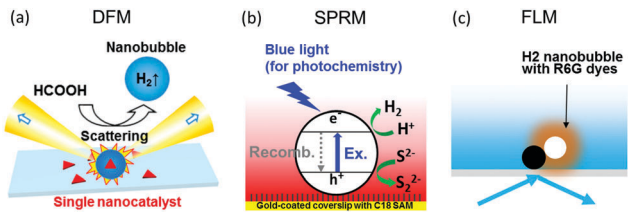

Fig. 10 The catalytic reaction occurring on a single nanoparticle is found to generate nano-sized gas bubbles on its surface. These nanobubbles can be visualized and quantified with DFM (a), SPRM (b) or FLM (c), allowing for the study of nanocatalysis at single-nanoparticle level. ((a) is reprinted with permission from ref. 233. Copyright 2017, American Chemical Society. (b) is reprinted with permission from ref. 17. Copyright 2017, National Academy of Science. (c) is modified with permission from ref. 294. Copyright 2018, Royal Society of Chemistry.)

Intermittent photocatalytic activity (photochemical blinking) of single CdS nanoparticles was observed in both cases, suggesting the intrinsic connection between semiconductor photophysics (blinking FL) and photochemistry (blinking photocatalysis). The major challenge is how to differentiate nucleation kinetics from intrinsic reaction kinetics, although they are likely to be correlated for the same nanocatalysts. However, for different nanocatalysts with different surface physiochemical properties and structures, bubble generation rates may not be sufficient to judge the catalytic activity.

Optical signal from nanocatalysts

In many cases, the optical signal of the nanocatalyst itself is sufficiently high to allow for tracing its trajectory during catalytic reactions. For instance, the scattering spectral band of a plasmonic nanoparticle is sensitively dependent on its electron density, which is subject to change due to electron injection or extraction during nanocatalysis. This mechanism was originally proposed by Mulvaney to investigate the oxidation of ascorbic acid.[81] Because it was difficult for conventional DFM to image metal nanocrystals smaller than 10 nm, which, however, often exhibited higher catalytic activity, Li developed a DNA-directed assembly strategy to form a core–satellite structure. Smaller satellite nanocrystals catalyzed the oxidation of glucose to inject electrons into the larger plasmonic core, leading to a detectable shift in the scattering spectrum.[82] The photo-induced reduction of 4-nitrobenzenethiols on single silver nanoparticles was investigated with DFM, which revealed a non-monotonic trend in the scattering intensity trajectory.[295] Bi-directional electron transfer in a Schottky junction was monitored in real time with SPRM by placing semiconductor nanoparticles onto a planar gold film.[113] Oxidation of sulfide ions in the solution caused the deposition of sulfur atoms onto the CdS nanoparticles under blue-light illumination. These sulfur atoms were reduced by hot electrons when the gold film was excited to generate surface plasmon polaritons. The reversible processes altered the dielectric constant of the CdS nanoparticles, which was indicated by the optical responses in SPRM. Long *et al.* examined the shift in scattering spectrum of a single gold nanorod when it catalyzed the electrochemical oxidation of H_2O_2. They attributed the observed red-shift to the formation of a hydroxide/oxide intermediate.[242,296] Photocatalysis of heavily doped titanium oxide nanomaterials was recently investigated under DFM.[297] Single-nanoparticle studies demonstrated that a nanoparticle dimer exhibited higher catalytic activity than an individual nanoparticle for photodegradation.

Ion-exchange reactions occurring on metal nanoparticles and semiconductor QDs were investigated with DFM and FLM, respectively. Metal-catalyzed galvanic replacement reactions are frequently utilized to synthesize bimetallic or hollow nanostructures, in which the corrosion of silver nanospheres by Au^{3+} results in gold nanocages. Monitoring the plasmonic spectrum of single silver nanoparticles not only confirmed the presence of nano-sized voids in the intermediate stage, but also revealed heterogeneous and rapid transition kinetics.[77] The spectral evolution of Ag nanoparticles in the presence of $[PtCl_6]^{2-}$ identified dynamic structural transformations for understanding the multi-domain Ag/AgCl/Pt nanostructure.[298] The single-nanoparticle trajectory further demonstrated that the surface ligands of the Ag nanoparticles played essential roles in regulating the galvanic replacement kinetics.[299] Metal ion exchange of CdSe nanoparticles by Ag^+ was found to eliminate the FL emission due to the formation of non-fluorescent Ag_2Se. A sharp transition as well as the narrow distribution of waiting times in the FL trajectories suggested that the ion exchange process was controlled by a cooperative phase transition mechanism.[300] In a reversed ion exchange process from Ag_2Se to CdSe, an intensified photoblinking pattern was detected during the FL recovery, uncovering an interesting correlation between the stochastic photoblinking and its chemical states.[60]

In addition to plasmonic scattering, the plasmonic photoluminescence of metal nanoparticles was also utilized to study nanocatalysis.[301] A single-nanoparticle PL spectrum can be acquired by using an optical microscope similar to a Raman microscope. It was further found that, similar to the plasmonic spectrum, the PL spectrum is also dependent on its geometry as well as the electron density,[302] allowing for the chemical processes to be probed. The PL spectrum of a single triangular gold nanoprism revealed the morphological evolution during an Au^{3+}-induced etching process.[303] Although the detailed mechanism of such plasmonic photoluminescence remains under debate,[50] a recent study reported the PL quenching as a result of an ethanol[49] and formic acid dehydrogenation reaction[304] occurring on it.

Perspective and outlook

Past decades have witnessed the rapid development of advanced optical microscopy with single-molecule detection sensitivity as well as an unprecedented spatial resolution that breaks the diffraction limit.[15,16] Applications in nanosensing, nanoelectrochemistry and nanocatalysis have not only significantly advanced fundamental knowledge about the optical properties and chemical activity of nanomaterials, but have also provided novel insights into the rational design of nanomaterials with better performance. While many exciting milestones and fruitful results have been demonstrated, further efforts are still required to reach the ultimate goals promised by single-nanoparticle studies. We summarize some of the remaining technical and conceptual challenges and provide our perspectives on future trends below.

From the point of view of technology, continuing attempts are expected to further improve the SBR of each imaging technique and to better mimic the actual reaction conditions. Improved SBR not only allows for the study of nanocatalysts of smaller size (which are often more chemically active), but also helps to achieve a higher temporal resolution. The latter is critical for nanocatalysis studies by reducing the influence of the diffusion of products and by probing fast kinetics. While FL and plasmonic nanomaterials have been deeply investigated by FLM and DFM, more attention to PTM and SPRM should be

encouraged because they are capable of studying broader types of nanomaterials for real-world applications. In most studies, a substrate is often required to facilitate the optical imaging of nanoparticles by eliminating Brownian motion. However, the presence of the substrate might alter the molecular recognition and electron transfer because of the hydrophilic–hydrophobic property, surface charge, roughness and electrical contact between nanoparticle and substrate. One of the solutions is to detach the nanoparticle from the substrate and to hold it with other non-contact techniques, such as optical and magnetic tweezers,[305–310] microcapsules, fluidics, or mechanical micromanipulators.[311] In addition, reaction chambers that are compatible with harsh temperature and pressure conditions are beneficial for expanding the applications.[7]

One of the ultimate goals promised by single-nanoparticle studies is to clarify the structure–activity relationship. Despite many exciting achievements towards this goal in the past two decades,[10,11] more examples are needed to show that microscopic studies lead directly to improved ensemble performances. The challenges are complicated, but we will try to list several solutions here. First, statistical analysis of thousands of (or even more) individuals are certainly required to deliver a reliable structure–activity relationship. While the activity of single nanoparticles has been convincingly determined, it is more difficult to extract one or a few structural features to build a relationship if the sample set is small.[233,264] Because each nanoparticle is so dramatically different from the others, it would be fanciful to use just a single structural feature (shape or size) to describe such heterogeneity. Comprehensive characterizations of single nanoparticles with multiple tools are required, including high-resolution and in-depth electron microscopes and scanning probe microscopes. In addition to the atomic structure, surface chemistry (adsorbates and defects) also plays a critical role in regulating chemical activity.[108,112] Unfortunately, *in situ* and single-nanoparticle-level characterizations on the surface chemistry of single nanoparticles are technically difficult. Because several structural features contributed to the chemical activity simultaneously, multiple parameter analysis of a sufficiently large sample set, rather than a single parameter from a few individual particles, is more likely to build a reliable structural–activity relationship. Statistical analysis is also critical because it might be able to explain the inconsistent and sometimes contradictory reports on the same or similar reaction system by surveying all the possible subpopulations.[243,312] Second, *in situ* manipulation of a single nanoparticle structure could be a powerful tool to clarify structural dependencies. Instead of simply measuring an existing nanoparticle, *in situ* modifications of its structure and observations of the consequences provide a more effective and convincing strategy. Available *in situ* manipulation methods include photochemical, electrochemical and chemical deposition, etching or corrosion, and assembly. A focused beam or an electrochemical probe enables further localized manipulation for a particular nanoparticle or a sub-nanoparticle location. This strategy is believed to be more efficient because such a perturbation and observation scheme represents a structural control experiment. It should be particularly useful for studying hybrid nanomaterials, such as co-catalysts. Third, a multifunctional system is needed to integrate the strengths of multiple imaging modes.[313,314] For example, it was found that the SERS background originated from the photoluminescence of plasmonic nanoparticles. Intrinsic SERS spectra were thus retrieved by removing the contribution of photoluminescence in a combined FLM and SERS system.[314] Spectroscopic measurements, such as FLM and PTM, revealed important information regarding surface trap states and electronic structures that are more relevant to chemical activity.[165] Attention should be paid in future work to correlating chemical activity with spectroscopic features, in addition to the structural dependencies.

Finally, since there have been versatile choices in the single-nanoparticle chemical imaging toolbox, we believe it is time to move to the next stage by building a stronger bond with ensemble measurements.[280,281] This includes two levels of meaning. First, it is anticipated that single-nanoparticle measurement will be able to reproduce and explain the activity trends in a series of ensemble samples. If sample A is 10 times more effective than sample B in an ensemble experiment, the same ratio should be expected when comparing the averaged activity of many individuals in single-nanoparticle measurements, no matter how much particle-to-particle heterogeneity is present. Second, it is anticipated that single-nanoparticle measurements will provide insights for improving performance and such guidance should be examined at the ensemble level. It is anticipated that further developments of optical imaging techniques, as well as strong interactions between single-entity measurements and ensemble experiments, will pave a solid way towards this ultimate goal.

Conflicts of interest

There are no conflicts to declare.

Acknowledgements

The author is grateful to financial support from the National Natural Science Foundation of China (Grants No. 21527807, 21522503 and 21327902), and the Natural Science Foundation of Jiangsu Province (BK20150013).

References

1 S. M. Nie, D. T. Chiu and R. N. Zare, *Science*, 1994, **266**, 1018–1021.
2 M. Nirmal, B. O. Dabbousi, M. G. Bawendi, J. J. Macklin, J. K. Trautman, T. D. Harris and L. E. Brus, *Nature*, 1996, **383**, 802–804.
3 S. Schultz, D. R. Smith, J. J. Mock and D. A. Schultz, *Proc. Natl. Acad. Sci. U. S. A.*, 2000, **97**, 996–1001.
4 S. M. Nie and S. R. Emery, *Science*, 1997, **275**, 1102–1106.
5 D. Boyer, P. Tamarat, A. Maali, B. Lounis and M. Orrit, *Science*, 2002, **297**, 1160–1163.

6 S. P. Wang, X. N. Shan, U. Patel, X. P. Huang, J. Lu, J. H. Li and N. J. Tao, *Proc. Natl. Acad. Sci. U. S. A.*, 2010, **107**, 16028–16032.
7 T. N. X. Ding, L. Hou, H. van der Meer, A. P. Alivisatos and M. Orrit, *J. Phys. Chem. Lett.*, 2016, **7**, 2524–2529.
8 J. O. Arroyo and P. Kukura, *Nat. Photonics*, 2016, **10**, 11–17.
9 T. Cordes and S. A. Blum, *Nat. Chem.*, 2013, **5**, 993–999.
10 M. B. J. Roeffaers, B. F. Sels, H. Uji-i, F. C. De Schryver, P. A. Jacobs, D. E. De Vos and J. Hofkens, *Nature*, 2006, **439**, 572–575.
11 J. B. Sambur, T. Y. Chen, E. Choudhary, G. Q. Chen, E. J. Nissen, E. M. Thomas, N. M. Zou and P. Chen, *Nature*, 2016, **530**, 77–80.
12 K. A. Willets, *Chem. Soc. Rev.*, 2014, **43**, 3854–3864.
13 R. M. Dickson, A. B. Cubitt, R. Y. Tsien and W. E. Moerner, *Nature*, 1997, **388**, 355–358.
14 P. Frantsuzov, M. Kuno, B. Janko and R. A. Marcus, *Nat. Phys.*, 2008, **4**, 519–522.
15 E. Betzig, G. H. Patterson, R. Sougrat, O. W. Lindwasser, S. Olenych, J. S. Bonifacino, M. W. Davidson, J. Lippincott-Schwartz and H. F. Hess, *Science*, 2006, **313**, 1642–1645.
16 M. J. Rust, M. Bates and X. W. Zhuang, *Nat. Methods*, 2006, **3**, 793–795.
17 Y. M. Fang, Z. M. Li, Y. Y. Jiang, X. Wang, H. Y. Chen, N. J. Tao and W. Wang, *Proc. Natl. Acad. Sci. U. S. A.*, 2017, **114**, 10566–10571.
18 H. P. Lu, L. Y. Xun and X. S. Xie, *Science*, 1998, **282**, 1877–1882.
19 W. L. Xu, J. S. Kong, Y. T. E. Yeh and P. Chen, *Nat. Mater.*, 2008, **7**, 992–996.
20 J. Y. Huang, L. Zhong, C. M. Wang, J. P. Sullivan, W. Xu, L. Q. Zhang, S. X. Mao, N. S. Hudak, X. H. Liu, A. Subramanian, H. Y. Fan, L. A. Qi, A. Kushima and J. Li, *Science*, 2010, **330**, 1515–1520.
21 Y. Takahashi, A. Kumatani, H. Shiku and T. Matsue, *Anal. Chem.*, 2017, **89**, 342–357.
22 A. Kumar, F. Ciucci, A. N. Morozovska, S. V. Kalinin and S. Jesse, *Nat. Chem.*, 2011, **3**, 707–713.
23 C. Y. Wu, W. J. Wolf, Y. Levartovsky, H. A. Bechtel, M. C. Martin, F. D. Toste and E. Gross, *Nature*, 2017, **541**, 511–515.
24 L. Xiao and Z. D. Schultz, *Anal. Chem.*, 2018, **90**, 440–458.
25 C. Joo, H. Balci, Y. Ishitsuka, C. Buranachai and T. Ha, *Annu. Rev. Biochem.*, 2008, **77**, 51–76.
26 A. S. Stender, K. Marchuk, C. Liu, S. Sander, M. W. Meyer, E. A. Smith, B. Neupane, G. F. Wang, J. J. Li, J. X. Cheng, B. Huang and N. Fang, *Chem. Rev.*, 2013, **113**, 2469–2527.
27 V. Ntziachristos, *Nat. Methods*, 2010, **7**, 603–614.
28 T. Ha and P. Tinnefeld, *Annu. Rev. Phys. Chem.*, 2012, **63**, 595–617.
29 K. Mathwig, T. J. Aartsma, G. W. Canters and S. G. Lemay, *Annu. Rev. Anal. Chem.*, 2014, **7**, 383–404.
30 A. B. Zrimsek, N. Chiang, M. Mattei, S. Zaleski, M. O. McAnally, C. T. Chapman, A.-I. Henry, G. C. Schatz and R. P. Van Duyne, *Chem. Rev.*, 2017, **117**, 7583–7613.
31 D. M. Jameson and J. A. Ross, *Chem. Rev.*, 2010, **110**, 2685–2708.
32 D. Axelrod, in *Biophysical Tools for Biologists, vol. 2: In Vivo Techniques*, ed. J. J. Correia and H. W. Detrich, 2008, vol. 89, pp. 169–221.
33 D. A. VandenBout, W. T. Yip, D. H. Hu, D. K. Fu, T. M. Swager and P. F. Barbara, *Science*, 1997, **277**, 1074–1077.
34 S. Wu, G. Han, D. J. Milliron, S. Aloni, V. Altoe, D. V. Talapin, B. E. Cohen and P. J. Schuck, *Proc. Natl. Acad. Sci. U. S. A.*, 2009, **106**, 10917–10921.
35 D. J. Gargas, E. M. Chan, A. D. Ostrowski, S. Aloni, M. V. P. Altoe, E. S. Barnard, B. Sanii, J. J. Urban, D. J. Milliron, B. E. Cohen and P. J. Schuck, *Nat. Nanotechnol.*, 2014, **9**, 300–305.
36 J. B. Zhao, D. Y. Jin, E. P. Schartner, Y. Q. Lu, Y. J. Liu, A. V. Zvyagin, L. X. Zhang, J. M. Dawes, P. Xi, J. A. Piper, E. M. Goldys and T. M. Monro, *Nat. Nanotechnol.*, 2013, **8**, 729–734.
37 Y.-S. Park, S. Guo, N. S. Makarov and V. I. Klimov, *ACS Nano*, 2015, **9**, 10386–10393.
38 Y. Tian, A. Merdasa, M. Peter, M. Abdellah, K. Zheng, C. S. Ponseca, T. Pullerits, A. Yartsev, V. Sundström and I. G. Scheblykin, *Nano Lett.*, 2015, **15**, 1603–1608.
39 X. Wen, A. Ho-Baillie, S. Huang, R. Sheng, S. Chen, H.-C. Ko and M. A. Green, *Nano Lett.*, 2015, **15**, 4644–4649.
40 C. Wu, T. Schneider, M. Zeigler, J. Yu, P. G. Schiro, D. R. Burnham, J. D. McNeill and D. T. Chiu, *J. Am. Chem. Soc.*, 2010, **132**, 15410–15417.
41 C. Wu and D. T. Chiu, *Angew. Chem., Int. Ed.*, 2013, **52**, 3086–3109.
42 D. A. Tsyboulski, S. M. Bachilo and R. B. Weisman, *Nano Lett.*, 2005, **5**, 975–979.
43 L. Cognet, D. A. Tsyboulski, J.-D. R. Rocha, C. D. Doyle, J. M. Tour and R. B. Weisman, *Science*, 2007, **316**, 1465.
44 A. Hartschuh, H. N. Pedrosa, L. Novotny and T. D. Krauss, *Science*, 2003, **301**, 1354.
45 I. Díez and R. H. Ras, *Advanced Fluorescence Reporters in Chemistry and Biology II*, Springer, 2010, pp. 307–332.
46 T. Vosch, Y. Antoku, J.-C. Hsiang, C. I. Richards, J. I. Gonzalez and R. M. Dickson, *Proc. Natl. Acad. Sci. U. S. A.*, 2007, **104**, 12616–12621.
47 M. Sakamoto, T. Tachikawa, M. Fujitsuka and T. Majima, *J. Am. Chem. Soc.*, 2009, **131**, 6–7.
48 H. L. Hu, H. G. Duan, J. K. W. Yang and Z. X. Shen, *ACS Nano*, 2012, **6**, 10147–10155.
49 Z. K. Zheng and T. Majima, *Angew. Chem., Int. Ed.*, 2016, **55**, 2879–2883.
50 K. Q. Lin, J. Yi, S. Hu, J. J. Sun, J. T. Zheng, X. Wang and B. Ren, *ACS Photonics*, 2016, **3**, 1248–1255.
51 M. J. Fernee, P. Tamarat and B. Lounis, *Chem. Soc. Rev.*, 2014, **43**, 1311–1337.
52 M. O. Dekaliuk, O. Viagin, Y. V. Malyukin and A. P. Demchenko, *Phys. Chem. Chem. Phys.*, 2014, **16**, 16075–16084.
53 R. E. Thompson, D. R. Larson and W. W. Webb, *Biophys. J.*, 2002, **82**, 2775–2783.

54 A. L. Efros and D. J. Nesbitt, *Nat. Nanotechnol.*, 2016, **11**, 661–671.
55 M. Kuno, D. P. Fromm, H. F. Hamann, A. Gallagher and D. J. Nesbitt, *J. Chem. Phys.*, 2001, **115**, 1028–1040.
56 F. Hu, Z. Cao, C. Zhang, X. Wang and M. Xiao, *Sci. Rep.*, 2015, **5**, 8898.
57 J. Si, S. Volkan-Kacso, A. Eltom, Y. Morozov, M. P. McDonald, M. Kuno and B. Janko, *Nano Lett.*, 2015, **15**, 4317–4321.
58 E. Zbydniewska, A. Duzynska, M. Popoff, D. Hourlier, S. Lenfant, J. Judek, M. Zdrojek and T. Melin, *Nano Lett.*, 2015, **15**, 6349–6356.
59 B. T. Ji, E. Giovanelli, B. Habert, P. Spinicelli, M. Nasilowski, X. Z. Xu, N. Lequeux, J. P. Hugonin, F. Marquier, J. J. Greffet and B. Dubertret, *Nat. Nanotechnol.*, 2015, **10**, 170–175.
60 A. L. Routzahn and P. K. Jain, *Nano Lett.*, 2015, **15**, 2504–2509.
61 S. Kuhn, U. Hakanson, L. Rogobete and V. Sandoghdar, *Phys. Rev. Lett.*, 2006, **97**, 017402.
62 A. Kinkhabwala, Z. F. Yu, S. H. Fan, Y. Avlasevich, K. Mullen and W. E. Moerner, *Nat. Photonics*, 2009, **3**, 654–657.
63 S. Schietinger, T. Aichele, H. Q. Wang, T. Nann and O. Benson, *Nano Lett.*, 2010, **10**, 134–138.
64 P. Lodahl, A. F. van Driel, I. S. Nikolaev, A. Irman, K. Overgaag, D. Vanmaekelbergh and W. L. Vos, *Nature*, 2004, **430**, 654–657.
65 R. Regmi, J. Berthelot, P. M. Winkler, M. Mivelle, J. Proust, F. Bedu, I. Ozerov, T. Begou, J. Lumeau, H. Rigneault, M. F. Garcia-Parajo, S. Bidault, J. Wenger and N. Bonod, *Nano Lett.*, 2016, **16**, 5143–5151.
66 D. Ratchford, F. Shafiei, S. Kim, S. K. Gray and X. Q. Li, *Nano Lett.*, 2011, **11**, 1049–1054.
67 P. Holzmeister, E. Pibiri, J. J. Schmied, T. Sen, G. P. Acuna and P. Tinnefeld, *Nat. Commun.*, 2014, **5**, 5356.
68 H. Cang, A. Labno, C. G. Lu, X. B. Yin, M. Liu, C. Gladden, Y. M. Liu and X. Zhang, *Nature*, 2011, **469**, 385–388.
69 C. Steuwe, M. Erdelyi, G. Szekeres, M. Csete, J. J. Baumberg, S. Mahajan and C. F. Kaminski, *Nano Lett.*, 2015, **15**, 3217–3223.
70 E. Johlin, J. Solari, S. A. Mann, J. Wang, T. S. Shimizu and E. C. Garnett, *Nat. Commun.*, 2016, **7**, 13950.
71 J. N. Anker, W. P. Hall, O. Lyandres, N. C. Shah, J. Zhao and R. P. Van Duyne, *Nat. Mater.*, 2008, **7**, 442–453.
72 A. Weigel, A. Sebesta and P. Kukura, *ACS Photonics*, 2014, **1**, 848–856.
73 J. M. Luther, P. K. Jain, T. Ewers and A. P. Alivisatos, *Nat. Mater.*, 2011, **10**, 361–366.
74 P. Zijlstra and M. Orrit, *Rep. Prog. Phys.*, 2011, **74**, 106401.
75 C. M. Hill and S. Pan, *J. Am. Chem. Soc.*, 2013, **135**, 17250–17253.
76 L.-X. Qin, Y. Li, D.-W. Li, C. Jing, B.-Q. Chen, W. Ma, A. Heyman, O. Shoseyov, I. Willner, H. Tian and Y.-T. Long, *Angew. Chem., Int. Ed.*, 2012, **51**, 140–144.
77 J. G. Smith, Q. Yang and P. K. Jain, *Angew. Chem., Int. Ed.*, 2014, **53**, 2867–2872.
78 Z. X. Chen, J. J. Li, X. Q. Chen, J. T. Cao, J. R. Zhang, Q. H. Min and J. J. Zhu, *J. Am. Chem. Soc.*, 2015, **137**, 1903–1908.
79 C. Novo, A. M. Funston, A. K. Gooding and P. Mulvaney, *J. Am. Chem. Soc.*, 2009, **131**, 14664–14666.
80 S. S. E. Collins, X. Z. Wei, T. G. McKenzie, A. M. Funston and P. Mulvaney, *Nano Lett.*, 2016, **16**, 6863–6869.
81 C. Novo, A. M. Funston and P. Mulvaney, *Nat. Nanotechnol.*, 2008, **3**, 598–602.
82 K. Li, K. Wang, W. W. Qin, S. H. Deng, D. Li, J. Y. Shi, Q. Huang and C. H. Fan, *J. Am. Chem. Soc.*, 2015, **137**, 4292–4295.
83 L. Lermusiaux, V. Maillard and S. Bidault, *ACS Nano*, 2015, **9**, 978–990.
84 Z. Gu, C. Jing, Y. L. Ying, P. G. He and Y. T. Long, *Theranostics*, 2015, **5**, 188–195.
85 J. R. Hao, B. Xiong, X. D. Chen, Y. He and E. S. Yeung, *Anal. Chem.*, 2014, **86**, 4663–4667.
86 J. Zhou, G. Lei, L. L. Zheng, P. F. Gao and C. Z. Huang, *Nanoscale*, 2016, **8**, 11467–11471.
87 B. Xiong, R. Zhou, J. R. Hao, Y. H. Jia, Y. He and E. S. Yeung, *Nat. Commun.*, 2013, **4**, 1708.
88 X. J. Liu, Q. Q. Zhang, Y. Tu, W. F. Zhao and H. W. Gai, *Anal. Chem.*, 2013, **85**, 11851–11857.
89 D. Zopf, J. Jatschka, A. Dathe, N. Jahr, W. Fritzsche and O. Stranik, *Biosens. Bioelectron.*, 2016, **81**, 287–293.
90 V. Pini, P. M. Kosaka, J. J. Ruz, O. Malvar, M. Encinar, J. Tamayo and M. Calleja, *Sci. Rep.*, 2016, **6**, 22836.
91 N. Fairbairn, A. Christofidou, A. G. Kanaras, T. A. Newman and O. L. Muskens, *Phys. Chem. Chem. Phys.*, 2013, **15**, 4163–4168.
92 P. Z. El-Khoury, A. G. Joly and W. P. Hess, *J. Phys. Chem. C*, 2016, **120**, 7295–7298.
93 M. A. Beuwer, M. W. J. Prins and P. Zijlstra, *Nano Lett.*, 2015, **15**, 3507–3511.
94 T. Kawawaki, H. Y. Zhang, H. Nishi, P. Mulvaney and T. Tatsuma, *J. Phys. Chem. Lett.*, 2017, **8**, 3637–3641.
95 I. Ament, J. Prasad, A. Henkel, S. Schmachtel and C. Soennichsen, *Nano Lett.*, 2012, **12**, 1092–1095.
96 L. O. Herrmann and J. J. Baumberg, *Small*, 2013, **9**, 3743–3747.
97 V. Wulf, F. Knoch, T. Speck and C. Sonnichsen, *J. Phys. Chem. Lett.*, 2016, **7**, 4951–4955.
98 C. Sonnichsen, S. Geier, N. E. Hecker, G. von Plessen, J. Feldmann, H. Ditlbacher, B. Lamprecht, J. R. Krenn, F. R. Aussenegg, V. Z. H. Chan, J. P. Spatz and M. Moller, *Appl. Phys. Lett.*, 2000, **77**, 2949–2951.
99 J. W. Ha, K. Marchuk and N. Fang, *Nano Lett.*, 2012, **12**, 4282–4288.
100 K. A. Koen, M. L. Weber, K. M. Mayer, E. Fernandez and K. A. Willets, *J. Phys. Chem. C*, 2012, **116**, 16198–16206.
101 K. Marchuk and N. Fang, *Nano Lett.*, 2013, **13**, 5414–5419.
102 J. Homola, *Chem. Rev.*, 2008, **108**, 462–493.
103 J. M. Pitarke, V. M. Silkin, E. V. Chulkov and P. M. Echenique, *Rep. Prog. Phys.*, 2007, **70**, 1–87.
104 B. Huang, F. Yu and R. N. Zare, *Anal. Chem.*, 2007, **79**, 2979–2983.

105 A. R. Halpern, J. B. Wood, Y. Wang and R. M. Corn, *ACS Nano*, 2014, **8**, 1022–1030.
106 I. Sidorenko, S. Nizamov, R. Hergenroder, A. Zybin, A. Kuzmichev, B. Kiwull, R. Niessner and V. M. Mirsky, *Microchim. Acta*, 2016, **183**, 101–109.
107 A. Zybin, Y. A. Kuritsyn, E. L. Gurevich, V. V. Temchura, K. Uberla and K. Niemax, *Plasmonics*, 2010, **5**, 31–35.
108 S. Nizamov, O. Kasian and V. M. Mirsky, *Angew. Chem., Int. Ed.*, 2016, **55**, 7247–7251.
109 S. Nizamov, V. Scherbahn and V. M. Mirsky, *Anal. Chem.*, 2016, **88**, 10206–10214.
110 V. Scherbahn, S. Nizamov and V. M. Mirsky, *Microchim. Acta*, 2016, **183**, 2837–2845.
111 X. N. Shan, I. Diez-Perez, L. J. Wang, P. Wiktor, Y. Gu, L. H. Zhang, W. Wang, J. Lu, S. P. Wang, Q. H. Gong, J. H. Li and N. J. Tao, *Nat. Nanotechnol.*, 2012, **7**, 668–672.
112 Y. M. Fang, W. Wang, X. Wo, Y. S. Luo, S. W. Yin, Y. X. Wang, X. N. Shan and N. J. Tao, *J. Am. Chem. Soc.*, 2014, **136**, 12584–12587.
113 Z. M. Li, Y. M. Fang, Y. J. Wang, Y. Y. Jiang, T. Liu and W. Wang, *Chem. Sci.*, 2017, **8**, 5019–5023.
114 D. Jiang, Y. Y. Jiang, Z. M. Li, T. Liu, X. Wo, Y. M. Fang, N. J. Tao, W. Wang and H. Y. Chen, *J. Am. Chem. Soc.*, 2017, **139**, 186–192.
115 X. Wo, Z. M. Li, Y. Y. Jiang, M. H. Li, Y. W. Su, W. Wang and N. J. Tao, *Anal. Chem.*, 2016, **88**, 2380–2385.
116 A. M. Maley, Y. Terada, S. Onogi, K. J. Shea, Y. Miura and R. M. Corn, *J. Phys. Chem. C*, 2016, **120**, 16843–16849.
117 K. Cho, J. B. Fasoli, K. Yoshimatsu, K. J. Shea and R. M. Corn, *Anal. Chem.*, 2015, **87**, 4973–4979.
118 K. Syal, S. M. Shen, Y. Z. Yang, S. P. Wang, S. E. Haydel and N. J. Tao, *ACS Sens.*, 2017, **2**, 1231–1239.
119 K. Syal, R. Iriya, Y. Z. Yang, H. Yu, S. P. Wang, S. E. Haydel, H. Y. Chen and N. J. Tao, *ACS Nano*, 2016, **10**, 845–852.
120 K. Syal, W. Wang, X. N. Shan, S. P. Wang, H. Y. Chen and N. J. Tao, *Biosens. Bioelectron.*, 2015, **63**, 131–137.
121 L. Viitala, A. M. Maley, H. W. M. Fung, R. M. Corn, T. Viitala and L. Murtomaki, *J. Phys. Chem. C*, 2016, **120**, 25958–25966.
122 Y. Z. Yang, H. Yu, X. N. Shan, W. Wang, X. W. Liu, S. P. Wang and N. J. Tao, *Small*, 2015, **11**, 2878–2884.
123 A. M. Maley, G. J. Lu, M. G. Shapiro and R. M. Corn, *ACS Nano*, 2017, **11**, 7447–7456.
124 L. Yuan, X. Wang, Y. M. Fang, C. B. Liu, D. Jiang, X. Wo, W. Wang and H. Y. Chen, *Anal. Chem.*, 2016, **88**, 2321–2326.
125 K. Cho, J. B. Fasoli, K. Yoshimatsu, K. J. Shea and R. M. Corn, *Anal. Chem.*, 2015, **87**, 4973–4979.
126 A. Demetriadou and A. A. Kornyshev, *New J. Phys.*, 2015, **17**, 013041.
127 A. Demetriadou, *Sci. Rep.*, 2015, **5**, 18247.
128 H. Yu, X. N. Shan, S. P. Wang, H. Y. Chen and N. J. Tao, *Anal. Chem.*, 2014, **86**, 8992–8997.
129 H. Yu, X. N. Shan, S. P. Wang and N. J. Tao, *Anal. Chem.*, 2017, **89**, 2704–2707.
130 C. Liu, C. F. Chan and H. C. Ong, *Opt. Commun.*, 2016, **378**, 28–34.
131 Z. X. Chen, X. N. Shan, Y. Guan, S. P. Wang, J. J. Zhu and N. J. Tao, *ACS Nano*, 2015, **9**, 11574–11581.
132 Y. M. Fang, S. Chen, W. Wang, X. N. Shan and N. J. Tao, *Angew. Chem., Int. Ed.*, 2015, **54**, 2538–2542.
133 X. N. Shan, Y. M. Fang, S. P. Wang, Y. Guan, H. Y. Chen and N. J. Tao, *Nano Lett.*, 2014, **14**, 4151–4157.
134 Y. M. Fang, H. Wang, H. Yu, X. W. Liu, W. Wang, H. Y. Chen and N. J. Tao, *Acc. Chem. Res.*, 2016, **49**, 2614–2624.
135 L. Yuan, N. J. Tao and W. Wang, *Annu. Rev. Anal. Chem.*, 2017, **10**, 183–200.
136 X. N. Shan, U. Patel, S. P. Wang, R. Iglesias and N. J. Tao, *Science*, 2010, **327**, 1363–1366.
137 W. Wang, K. Foley, X. Shan, S. P. Wang, S. Eaton, V. J. Nagaraj, P. Wiktor, U. Patel and N. J. Tao, *Nat. Chem.*, 2011, **3**, 249–255.
138 A. J. J. Jebaraj and D. A. Scherson, *Acc. Chem. Res.*, 2013, **46**, 1192–1205.
139 B. Redding, M. J. Schwab and Y. L. Pan, *Sensors*, 2015, **15**, 19021–19046.
140 K. Kneipp, Y. Wang, H. Kneipp, L. T. Perelman, I. Itzkan, R. Dasari and M. S. Feld, *Phys. Rev. Lett.*, 1997, **78**, 1667–1670.
141 X. Wang, S. C. Huang, T. X. Huang, H. S. Su, J. H. Zhong, Z. C. Zeng, M. H. Li and B. Ren, *Chem. Soc. Rev.*, 2017, **46**, 4020–4041.
142 J. Reguera, J. Langer, D. J. de Aberasturi and L. M. Liz-Marzan, *Chem. Soc. Rev.*, 2017, **46**, 3866–3885.
143 S. Y. Ding, E. M. You, Z. Q. Tian and M. Moskovits, *Chem. Soc. Rev.*, 2017, **46**, 4042–4076.
144 R. Zhang, Y. Zhang, Z. C. Dong, S. Jiang, C. Zhang, L. G. Chen, L. Zhang, Y. Liao, J. Aizpurua, Y. Luo, J. L. Yang and J. G. Hou, *Nature*, 2013, **498**, 82–86.
145 B. Sharma, R. R. Frontiera, A. I. Henry, E. Ringe and R. P. Van Duyne, *Mater. Today*, 2012, **15**, 16–25.
146 S. M. Stranahan and K. A. Willets, *Nano Lett.*, 2010, **10**, 3777–3784.
147 M. L. Weber and K. A. Willets, *J. Phys. Chem. Lett.*, 2011, **2**, 1766–1770.
148 C. Farcau and S. Astilean, *J. Phys. Chem. C*, 2010, **114**, 11717–11722.
149 J. F. Li, Y. F. Huang, Y. Ding, Z. L. Yang, S. B. Li, X. S. Zhou, F. R. Fan, W. Zhang, Z. Y. Zhou, D. Y. Wu, B. Ren, Z. L. Wang and Z. Q. Tian, *Nature*, 2010, **464**, 392–395.
150 A. J. Wright, J. L. Richens, J. P. Bramble, N. Cathcart, V. Kitaev, P. O'Shea and A. J. Hudson, *Nanoscale*, 2016, **8**, 16395–16404.
151 M. Takase, H. Ajiki, Y. Mizumoto, K. Komeda, M. Nara, H. Nabika, S. Yasuda, H. Ishihara and K. Murakoshi, *Nat. Photonics*, 2013, **7**, 550–554.
152 S. Yasuda, S. Hoshina, S. Chiashi, S. Maruyama and K. Murakoshi, *Nanoscale*, 2016, **8**, 19093–19098.
153 S. Mubeen, S. P. Zhang, N. Kim, S. Lee, S. Kramer, H. X. Xu and M. Moskovits, *Nano Lett.*, 2012, **12**, 2088–2094.

154 H. K. Lee, Y. H. Lee, J. V. Morabito, Y. J. Liu, C. S. L. Koh, I. Y. Phang, S. Pedireddy, X. M. Han, L. Y. Chou, C. K. Tsung and X. Y. Ling, *J. Am. Chem. Soc.*, 2017, **139**, 11513–11518.
155 Y. S. Yamamoto and T. Itoh, *J. Raman Spectrosc.*, 2016, **47**, 78–88.
156 S. R. Emory, R. A. Jensen, T. Wenda, M. Y. Han and S. M. Nie, *Faraday Discuss.*, 2006, **132**, 249–259.
157 Z. J. Wang and L. J. Rothberg, *J. Phys. Chem. B*, 2005, **109**, 3387–3391.
158 Y. Kitahama, T. Nagahiro, Y. Tanaka, T. Itoh and Y. Ozaki, *J. Raman Spectrosc.*, 2017, **48**, 570–577.
159 J. R. Lombardi, R. L. Birke and G. Haran, *J. Phys. Chem. C*, 2011, **115**, 4540–4545.
160 T. Itoh and Y. S. Yamamoto, *Analyst*, 2016, **141**, 5000–5009.
161 P. B. Joshi, T. P. Anthony, A. J. Wilson and K. A. Willets, *Faraday Disc.*, 2017, **205**, 245–259.
162 L. Cognet, S. Berciaud, D. Lasne and B. Lounis, *Anal. Chem.*, 2008, **80**, 2288–2294.
163 S. Berciaud, L. Cognet and B. Lounis, *Nano Lett.*, 2005, **5**, 2160–2163.
164 J. Giblin, M. Syed, M. T. Banning, M. Kuno and G. Hartland, *ACS Nano*, 2010, **4**, 358–364.
165 S. Berciaud, L. Cognet, P. Poulin, R. B. Weisman and B. Lounis, *Nano Lett.*, 2007, **7**, 1203–1207.
166 Z. Gao, L. Oudjedi, R. Faes, F. Morote, C. Jaillet, P. Poulin, B. Lounis and L. Cognet, *Sci. Rep.*, 2015, **5**, 17093.
167 J. Russier, L. Oudjedi, M. Piponnier, C. Bussy, M. Prato, K. Kostarelos, B. Lounis, A. Bianco and L. Cognet, *Nanoscale*, 2017, **9**, 4642–4645.
168 W.-S. Chang, J. W. Ha, L. S. Slaughter and S. Link, *Proc. Natl. Acad. Sci. U. S. A.*, 2010, **107**, 2781–2786.
169 S. Berciaud, L. Cognet, G. A. Blab and B. Lounis, *Phys. Rev. Lett.*, 2004, **93**, 257402.
170 A. Gaiduk, M. Yorulmaz, P. V. Ruijgrok and M. Orrit, *Science*, 2010, **330**, 353–356.
171 L. H. Xiao, J. W. Ha, L. Wei, G. F. Wang and N. Fang, *Angew. Chem., Int. Ed.*, 2012, **51**, 7734–7738.
172 K. Chen, Y. Gu, W. Sun, B. Dong, G. Wang, X. Fan, T. Xia and N. Fang, *Nat. Commun.*, 2017, **8**, 887.
173 Y. Luo, W. Sun, Y. Gu, G. F. Wang and N. Fang, *Anal. Chem.*, 2010, **82**, 6675–6679.
174 A. E. Augspurger, A. S. Stender, R. Han and N. Fang, *Anal. Chem.*, 2014, **86**, 1196–1201.
175 J. Ortega-Arroyo and P. Kukura, *Phys. Chem. Chem. Phys.*, 2012, **14**, 15625–15636.
176 P. Kukura, H. Ewers, C. Muller, A. Renn, A. Helenius and V. Sandoghdar, *Nat. Methods*, 2009, **6**, U923–U985.
177 P. Kukura, M. Celebrano, A. Renn and V. Sandoghdar, *Nano Lett.*, 2009, **9**, 926–929.
178 J. O. Arroyo, J. Andrecka, K. M. Spillane, N. Billington, Y. Takagi, J. R. Sellers and P. Kukura, *Nano Lett.*, 2014, **14**, 2065–2070.
179 D. Cole, G. Young, A. Weigel, A. Sebesta and P. Kukura, *ACS Photonics*, 2017, **4**, 211–216.
180 M. Piliarik and V. Sandoghdar, *Nat. Commun.*, 2014, **5**, 4495.
181 J. Andrecka, J. O. Arroyo, Y. Takagi, G. de Wit, A. Fineberg, L. MacKinnon, G. Young, J. R. Sellers and P. Kukura, *eLife*, 2015, **4**, e05413.
182 J. Cui, A. P. Beyler, L. F. Marshall, O. Chen, D. K. Harris, D. D. Wanger, X. Brokmann and M. G. Bawendi, *Nat. Chem.*, 2013, **5**, 602–606.
183 X. Chen, Q. Xia, Y. Cao, Q. Min, J. Zhang, Z. Chen, H.-Y. Chen and J.-J. Zhu, *Nat. Commun.*, 2017, **8**, 1498.
184 W. Wang and N. Tao, *Anal. Chem.*, 2014, **86**, 2–14.
185 L. Xiao and E. S. Yeung, *Annu. Rev. Anal. Chem.*, 2014, **7**, 89–111.
186 Y. Li, C. Jing, L. Zhang and Y.-T. Long, *Chem. Soc. Rev.*, 2012, **41**, 632–642.
187 J. Pan, F. Li and J. H. Choi, *J. Mater. Chem. B*, 2017, **5**, 6511–6522.
188 Y. Peng, B. Xiong, L. Peng, H. Li, Y. He and E. S. Yeung, *Anal. Chem.*, 2015, **87**, 200–215.
189 L. H. Guo, A. R. Ferhan, K. Lee and D. H. Kim, *Anal. Chem.*, 2011, **83**, 2605–2612.
190 S. M. E. Peters, M. A. Verheijen, M. W. J. Prins and P. Zijlstra, *Nanotechnology*, 2016, **27**, 024001.
191 T. Xie, C. Jing and Y. T. Long, *Analyst*, 2017, **142**, 409–420.
192 M. Sriram, K. Zong, S. R. C. Vivekchand and J. J. Gooding, *Sensors*, 2015, **15**, 25774–25792.
193 T. Li, X. Wu, F. Liu and N. Li, *Analyst*, 2017, **142**, 248–256.
194 A. D. McFarland and R. P. Van Duyne, *Nano Lett.*, 2003, **3**, 1057–1062.
195 Y. Y. Tian, L. Zhang, J. J. Shen, L. Z. Wu, H. Z. He, D. L. Ma, C. H. Leung, W. B. Wu, Q. L. Fan, W. Huang and L. H. Wang, *Small*, 2016, **12**, 2913–2920.
196 L. Zhang, J. H. Wang, J. X. Zhang, Y. Q. Liu, L. Z. Wu, J. J. Shen, Y. Zhang, Y. L. Hu, Q. L. Fan, W. Huang and L. H. Wang, *ACS Sens.*, 2017, **2**, 1435–1440.
197 G. L. Liu, Y. T. Long, Y. Choi, T. Kang and L. P. Lee, *Nat. Methods*, 2007, **4**, 1015–1017.
198 Y. Choi, Y. Park, T. Kang and L. P. Lee, *Nat. Nanotechnol.*, 2009, **4**, 742–746.
199 L. Shi, C. Jing, Z. Gu and Y. T. Long, *Sci. Rep.*, 2015, **5**.
200 Y. Kim, J. Y. Park, H. Y. Kim, M. Lee, J. Yi and I. Choi, *Chem. Commun.*, 2015, **51**, 15370–15373.
201 N. Liu, M. L. Tang, M. Hentschel, H. Giessen and A. P. Alivisatos, *Nat. Mater.*, 2011, **10**, 631–636.
202 L. Zhang, Y. Li, D. W. Li, C. Jing, X. Y. Chen, M. Lv, Q. Huang, Y. T. Long and I. Willner, *Angew. Chem., Int. Ed.*, 2011, **50**, 6789–6792.
203 S. Chen, M. Svedendahl, R. P. Van Duyne and M. Kall, *Nano Lett.*, 2011, **11**, 1826–1830.
204 C. Sonnichsen, B. M. Reinhard, J. Liphardt and A. P. Alivisatos, *Nat. Biotechnol.*, 2005, **23**, 741–745.
205 B. Xiong, Z. R. Huang, H. Y. Zou, C. Y. Qiao, Y. He and E. S. Yeung, *ACS Nano*, 2017, **11**, 541–548.
206 Q. Liu, C. Jing, X. X. Zheng, Z. Gu, D. Li, D. W. Li, Q. Huang, Y. T. Long and C. H. Fan, *Chem. Commun.*, 2012, **48**, 9574–9576.
207 L. Shi, C. Jing, W. Ma, D.-W. Li, J. E. Halls, F. Marken and Y.-T. Long, *Angew. Chem., Int. Ed.*, 2013, **52**, 6011–6014.

208 V. V. Thacker, L. O. Herrmann, D. O. Sigle, T. Zhang, T. Liedl, J. J. Baumberg and U. F. Keyser, *Nat. Commun.*, 2014, **5**, 3448.
209 L. Weller, V. V. Thacker, L. O. Herrmann, E. A. Hemmig, A. Lombardi, U. F. Keyser and J. J. Baumberg, *ACS Photonics*, 2016, **3**, 1589–1595.
210 A. Gaiduk, P. V. Ruijgrok, M. Yorulmaz and M. Orrit, *Chem. Sci.*, 2010, **1**, 343–350.
211 H. Yu, X. N. Shan, S. P. Wang, H. Y. Chen and N. J. Tao, *ACS Nano*, 2014, **8**, 3427–3433.
212 D. Cole, G. Young, A. Weigel, A. Sebesta and P. Kukura, *ACS Photonics*, 2017, **4**, 211–216.
213 N. Zhang, Y. J. Liu, J. Yang, X. D. Su, J. Deng, C. C. Chum, M. H. Hong and J. H. Teng, *Nanoscale*, 2014, **6**, 1416–1422.
214 P. Zijlstra, P. M. R. Paulo and M. Orrit, *Nat. Nanotechnol.*, 2012, **7**, 379–382.
215 M. D. Baaske and F. Vollmer, *Nat. Photonics*, 2016, **10**, 733–739.
216 W. Wang, *Sci. Bull.*, 2015, **60**, 1866–1867.
217 R. E. Palacios, F.-R. F. Fan, J. K. Grey, J. Suk, A. J. Bard and P. F. Barbara, *Nat. Mater.*, 2007, **6**, 680–685.
218 J. M. Salverda, A. V. Patil, G. Mizzon, S. Kuznetsova, G. Zauner, N. Akkilic, G. W. Canters, J. J. Davis, H. A. Heering and T. J. Aartsma, *Angew. Chem., Int. Ed.*, 2010, **49**, 5776–5779.
219 L. Bouffier and T. Doneux, *Curr. Opin. Electrochem.*, 2017, **6**, 31–37.
220 C. Jing and J. Reichert, *Curr. Opin. Electrochem.*, 2017, **6**, 10–16.
221 T. Yuan and W. Wang, *Curr. Opin. Electrochem.*, 2017, **6**, 17–22.
222 L. L. Sun, D. Jiang, M. Li, T. Liu, L. Yuan, W. Wang and H. Y. Chen, *Anal. Chem.*, 2017, **89**, 6051–6056.
223 Y. X. Wang, X. N. Shan, H. Wang, S. P. Wang and N. J. Tao, *J. Am. Chem. Soc.*, 2017, **139**, 1376–1379.
224 D. Jiang, L. Sun, T. Liu and W. Wang, *Anal. Chem.*, 2017, **89**, 11641–11647.
225 C. Batchelor-McAuley, C. A. Little, S. V. Sokolov, E. Katelhon, G. Zampardi and R. G. Compton, *Anal. Chem.*, 2016, **88**, 11213–11221.
226 J. G. Wang, J. S. Fossey, M. Li, T. Xie and Y. T. Long, *ACS Appl. Mater. Interfaces*, 2016, **8**, 8305–8314.
227 C. M. Hill, R. Bennett, C. Zhou, S. Street, J. Zheng and S. L. Pan, *J. Phys. Chem. C*, 2015, **119**, 6760–6768.
228 A. N. Patel, A. Martinez-Marrades, V. Brasiliense, D. Koshelev, M. Besbes, R. Kuszelewicz, C. Combellas, G. Tessier and F. Kanoufi, *Nano Lett.*, 2015, **15**, 6454–6463.
229 S. E. Fosdick, M. J. Anderson, E. G. Nettleton and R. M. Crooks, *J. Am. Chem. Soc.*, 2013, **135**, 5994–5997.
230 V. Brasiliense, A. N. Patel, A. Martinez-Marrades, J. Shi, Y. Chen, C. Combellas, G. Tessier and F. Kanoufi, *J. Am. Chem. Soc.*, 2016, **138**, 3478–3483.
231 L. Sun, Y. Fang, Z. Li, W. Wang and H. Chen, *Nano Res.*, 2017, **10**, 1740–1748.
232 A. J. Wilson and K. A. Willets, *Nano Lett.*, 2014, **14**, 939–945.
233 S. Li, Y. Du, T. He, Y. Shen, C. Bai, F. Ning, W. Wang, S. Xi and X. Zhou, *J. Am. Chem. Soc.*, 2017, **139**, 14277–14284.
234 M. Chirea, S. S. E. Collins, X. Wei and P. Mulvaney, *J. Phys. Chem. Lett.*, 2014, **5**, 4331–4335.
235 A. J. Wilson, K. Marchuk and K. A. Willets, *Nano Lett.*, 2015, **15**, 6110–6115.
236 S. Pan, J. Liu and C. M. Hill, *J. Phys. Chem. C*, 2015, **119**, 27095–27103.
237 M.-J. Zhu, J.-B. Pan, Z.-Q. Wu, X.-Y. Gao, W. Zhao, X.-H. Xia, J.-J. Xu and H.-Y. Chen, *Angew. Chem., Int. Ed.*, 2018, **57**, DOI: 10.1002/anie.201800706.
238 H. Zhou, Q. Liu, F. J. Rawson, W. Ma, D. W. Li, D. Li and Y. T. Long, *Chem. Commun.*, 2015, **51**, 3223–3226.
239 S. K. Dondapati, M. Ludemann, R. Mueller, S. Schwieger, A. Schwemer, B. Haendel, D. Kwiatkowski, M. Djiango, E. Runge and T. A. Klar, *Nano Lett.*, 2012, **12**, 1247–1252.
240 C. P. Byers, B. S. Hoener, W.-S. Chang, S. Link and C. F. Landes, *Nano Lett.*, 2016, **16**, 2314–2321.
241 A. B. Dahlin, R. Zahn and J. Voeroes, *Nanoscale*, 2012, **4**, 2339–2351.
242 C. Jing, F. J. Rawson, H. Zhou, X. Shi, W.-H. Li, D.-W. Li and Y.-T. Long, *Anal. Chem.*, 2014, **86**, 5513–5518.
243 C. P. Byers, B. S. Hoener, W.-S. Chang, M. Yorulmaz, S. Link and C. F. Landes, *J. Phys. Chem. B*, 2014, **118**, 14047–14055.
244 A. X. Yin, Q. Y. He, Z. Y. Lin, L. Luo, Y. Liu, S. Yang, H. Wu, M. N. Ding, Y. Huang and X. F. Duan, *Angew. Chem., Int. Ed.*, 2016, **55**, 583–587.
245 H. Wang, X. Shan, H. Yu, Y. Wang, W. Schmickler, H. Y. Chen and N. Tao, *Angew. Chem., Int. Ed.*, 2017, **56**, 2132–2135.
246 X. N. Shan, S. Chen, H. Wang, Z. X. Chen, Y. Guan, Y. X. Wang, S. P. Wang, H. Y. Chen and N. J. Tao, *Adv. Mater.*, 2015, **27**, 6213–6219.
247 H. Wang, X. N. Shan, H. Y. Chen and N. J. Tao, *Nano Lett.*, 2017, **17**, 236–241.
248 M. W. Holman, R. C. Liu and D. M. Adams, *J. Am. Chem. Soc.*, 2003, **125**, 12649–12654.
249 W. C. Zhang, M. Caldarola, B. Pradhan and M. Orrit, *Angew. Chem., Int. Ed.*, 2017, **56**, 3566–3569.
250 J. Lu, Y. S. Fan, M. D. Howard, J. C. Vaughan and B. Zhang, *J. Am. Chem. Soc.*, 2017, **139**, 2964–2971.
251 W. Xu, H. Shen, Y. J. Kim, X. Zhou, G. Liu, J. Park and P. Chen, *Nano Lett.*, 2009, **9**, 3968–3973.
252 E. Cortes, P. G. Etchegoin, E. C. Le Ru, A. Fainstein, M. E. Vela and R. C. Salvarezza, *J. Am. Chem. Soc.*, 2010, **132**, 18034–18037.
253 E. Cortes, P. G. Etchegoin, E. C. Le Ru, A. Fainstein, M. E. Vela and R. C. Salvarezza, *J. Am. Chem. Soc.*, 2013, **135**, 2809–2815.
254 C. M. Hill, D. A. Clayton and S. Pan, *Phys. Chem. Chem. Phys.*, 2013, **15**, 20797–20807.
255 J. B. Sambur and P. Chen, *Annu. Rev. Phys. Chem.*, 2014, **65**, 395–422.
256 T. Tachikawa and T. Majima, *Chem. Soc. Rev.*, 2010, **39**, 4802–4819.

257 K. P. F. Janssen, G. De Cremer, R. K. Neely, A. V. Kubarev, J. Van Loon, J. A. Martens, D. E. De Vos, M. B. J. Roeffaers and J. Hofkens, *Chem. Soc. Rev.*, 2014, **43**, 990–1006.
258 T. Chen, B. Dong, K. Chen, F. Zhao, X. Cheng, C. Ma, S. Lee, P. Zhang, S. H. Kang, J. W. Ha, W. Xu and N. Fang, *Chem. Rev.*, 2017, **117**, 7510–7537.
259 P. Chen, X. C. Zhou, N. M. Andoy, K. S. Han, E. Choudhary, N. M. Zou, G. Q. Chen and H. Shen, *Chem. Soc. Rev.*, 2014, **43**, 1107–1117.
260 X. Zhou, N. M. Andoy, G. Liu, E. Choudhary, K.-S. Han, H. Shen and P. Chen, *Nat. Nanotechnol.*, 2012, **7**, 237–241.
261 R. Han, J. W. Ha, C. X. Xiao, Y. C. Pei, Z. Y. Qi, B. Dong, N. L. Bormann, W. Y. Huang and N. Fang, *Angew. Chem., Int. Ed.*, 2014, **53**, 12865–12869.
262 T. Chen, Y. W. Zhang and W. L. Xu, *J. Am. Chem. Soc.*, 2016, **138**, 12414–12421.
263 Y. W. Zhang, P. Song, Q. Fu, M. B. Ruan and W. L. Xu, *Nat. Commun.*, 2014, **5**, 4238.
264 X. C. Zhou, E. Choudhary, N. M. Andoy, N. M. Zou and P. Chen, *ACS Catal.*, 2013, **3**, 1448–1453.
265 T. Chen, S. Chen, P. Song, Y. W. Zhang, H. Y. Su, W. L. Xu and J. Zeng, *ACS Catal.*, 2017, **7**, 2967–2972.
266 Z. Ristanovic, A. V. Kubarev, J. Hofkens, M. B. J. Roeffaers and B. M. Weckhuysen, *J. Am. Chem. Soc.*, 2016, **138**, 13586–13596.
267 T. Chen, Y. W. Zhang and W. L. Xu, *Phys. Chem. Chem. Phys.*, 2016, **18**, 22494–22502.
268 T. Chen, S. Chen, Y. W. Zhang, Y. F. Qi, Y. Z. Zhao, W. L. Xu and J. Zeng, *Angew. Chem., Int. Ed.*, 2016, **55**, 1839–1843.
269 N. M. Andoy, X. C. Zhou, E. Choudhary, H. Shen, G. K. Liu and P. Chen, *J. Am. Chem. Soc.*, 2013, **135**, 1845–1852.
270 J. W. Ha, T. P. A. Ruberu, R. Han, B. Dong, J. Vela and N. Fang, *J. Am. Chem. Soc.*, 2014, **136**, 1398–1408.
271 Y. W. Zhang, J. M. Lucas, P. Song, B. Beberwyck, Q. Fu, W. L. Xu and A. P. Alivisatos, *Proc. Natl. Acad. Sci. U. S. A.*, 2015, **112**, 8959–8964.
272 Y. W. Zhang, T. Chen, S. Alia, B. S. Pivovar and W. L. Xu, *Angew. Chem., Int. Ed.*, 2016, **55**, 3086–3090.
273 F. C. Hendriks, S. Mohammadian, Z. Ristanović, S. Kalirai, F. Meirer, E. T. Vogt, P. C. Bruijnincx, H. C. Gerritsen and B. M. Weckhuysen, *Angew. Chem., Int. Ed.*, 2018, **57**, 257–261.
274 T. Tachikawa, S. Yamashita and T. Majima, *J. Am. Chem. Soc.*, 2011, **133**, 7197–7204.
275 X. C. Zhou, W. L. Xu, G. K. Liu, D. Panda and P. Chen, *J. Am. Chem. Soc.*, 2010, **132**, 138–146.
276 V. G. Rao, B. Dhital, Y. He and H. P. Lu, *J. Phys. Chem. C*, 2014, **118**, 20209–20221.
277 N. M. Esfandiari and S. A. Blum, *J. Am. Chem. Soc.*, 2011, **133**, 18145–18147.
278 M. R. Decan, S. Impellizzeri, M. L. Marin and J. C. Scaiano, *Nat. Commun.*, 2014, **5**, 4612.
279 G. K. Hodgson, S. Impellizzeri and J. C. Scaiano, *Catal. Sci. Technol.*, 2016, **6**, 7113–7121.
280 G. K. Hodgson, S. Impellizzeri and J. C. Scaiano, *Chem. Sci.*, 2016, **7**, 1314–1321.
281 Z. Ristanovic, J. P. Hofmann, G. De Cremer, A. V. Kubarev, M. Rohnke, F. Meirer, J. Hofkens, M. B. J. Roeffaers and B. M. Weckhuysen, *J. Am. Chem. Soc.*, 2015, **137**, 6559–6568.
282 T.-L. E. Wee, L. C. Schmidt and J. C. Scaiano, *J. Phys. Chem. C*, 2012, **116**, 24373–24379.
283 E. M. van Schrojenstein Lantman, T. Deckert-Gaudig, A. J. G. Mank, V. Deckert and B. M. Weckhuysen, *Nat. Nanotechnol.*, 2012, **7**, 583–586.
284 J. H. Zhong, X. Jin, L. Y. Meng, X. Wang, H. S. Su, Z. L. Yang, C. T. Williams and B. Ren, *Nat. Nanotechnol.*, 2017, **12**, 132–136.
285 E. M. V. Lantman, P. de Peinder, A. J. G. Mank and B. M. Weckhuysen, *ChemPhysChem*, 2015, **16**, 547–554.
286 H. K. Choi, W. H. Park, C. G. Park, H. H. Shin, K. S. Lee and Z. H. Kirn, *J. Am. Chem. Soc.*, 2016, **138**, 4673–4684.
287 B. de Nijs, F. Benz, S. J. Barrow, D. O. Sigle, R. Chikkaraddy, A. Palma, C. Carnegie, M. Kamp, R. Sundararaman, P. Narang, O. A. Scherman and J. J. Baumberg, *Nat. Commun.*, 2017, **8**, 994.
288 H. K. Choi, K. S. Lee, H. H. Shin and Z. H. Kim, *J. Phys. Chem. Lett.*, 2016, **7**, 4099–4104.
289 Z. L. Zhang, T. Deckert-Gaudig, P. Singh and V. Deckert, *Chem. Commun.*, 2015, **51**, 3069–3072.
290 M. L. Weber, A. J. Wilson and K. A. Willets, *J. Phys. Chem. C*, 2015, **119**, 18591–18601.
291 S. Zaleski, M. F. Cardinal, D. V. Chulhai, A. J. Wilson, K. A. Willets, L. Jensen and R. P. Van Duyne, *J. Phys. Chem. C*, 2016, **120**, 24982–24991.
292 Y.-F. Huang, M. Zhang, L.-B. Zhao, J.-M. Feng, D.-Y. Wu, B. Ren and Z.-Q. Tian, *Angew. Chem., Int. Ed.*, 2014, **53**, 2353–2357.
293 D. Seo, G. Park and H. Song, *J. Am. Chem. Soc.*, 2012, **134**, 1221–1227.
294 H. Su, Y. Fang, F. Chen and W. Wang, *Chem. Sci.*, 2018, **9**, 1448–1453.
295 G. Lei, P. F. Gao, T. Yang, J. Zhou, H. Z. Zhang, S. S. Sun, M. X. Gao and C. Z. Huang, *ACS Nano*, 2017, **11**, 2085–2093.
296 C. Jing, Z. Gu and Y.-T. Long, *Faraday Disc.*, 2016, **193**, 371–385.
297 J. H. Yan, Z. Y. Lin, C. R. Ma, Z. Q. Zheng, P. Liu and G. W. Yang, *Nanoscale*, 2016, **8**, 15001–15007.
298 J. G. Smith, I. Chakraborty and P. K. Jain, *Angew. Chem., Int. Ed.*, 2016, **55**, 9979–9983.
299 J. G. Smith and P. K. Jain, *J. Am. Chem. Soc.*, 2016, **138**, 6765–6773.
300 A. L. Routzahn and P. K. Jain, *Nano Lett.*, 2014, **14**, 987–992.
301 Z. K. Zheng, T. Tachikawa and T. Majima, *J. Am. Chem. Soc.*, 2014, **136**, 6870–6873.
302 Z. Z. Lou, M. Fujitsuka and T. Majima, *ACS Nano*, 2016, **10**, 6299–6305.
303 Z. Z. Lou, S. Kim, P. Zhang, X. W. Shi, M. Fujitsuka and T. Majima, *ACS Nano*, 2017, **11**, 968–974.
304 Z. K. Zheng, T. Tachikawa and T. Majima, *J. Am. Chem. Soc.*, 2015, **137**, 948–957.
305 K. Pearce, F. Wang and P. J. Reece, *Opt. Exp.*, 2011, **19**, 25559–25569.
306 X. J. Gong, L. Hua, C. Wu and T. Ngai, *Rev. Sci. Instrum.*, 2013, **84**, 033702.

307 E. Suraniti, F. Kanoufi, C. Gosse, X. Zhao, R. Dimova, B. Pouligny and N. Sojic, *Anal. Chem.*, 2013, **85**, 8902–8909.
308 H. T. Xu, S. Jones, B. C. Choi and R. Gordon, *Nano Lett.*, 2016, **16**, 2639–2643.
309 M. Y. Wu, D. X. Ling, L. Ling, W. Li and Y. Q. Li, *Sci. Rep.*, 2017, **7**, 42930.
310 C. Liu, K. Kubo, E. Wang, K.-S. Han, F. Yang, G. Chen, F. A. Escobedo, G. W. Coates and P. Chen, *Science*, 2017, **358**, 352–355.
311 Y. Yu, V. Sundaresan, S. Bandyopadhyay, Y. Zhang, M. A. Edwards, K. McKelvey, H. S. White and K. A. Willets, *ACS Nano*, 2017, **11**, 10529–10538.
312 T. He, Y. Du, P. Y. Xu, S. B. Xi, Y. B. Shen, W. H. Ni, B. H. Yue and X. C. Zhou, *Small*, 2016, **12**, 5049–5057.
313 A. Tcherniak, J. W. Ha, S. Dominguez-Medina, L. S. Slaughter and S. Link, *Nano Lett.*, 2010, **10**, 1398–1404.
314 K. Q. Lin, J. Yi, J. H. Zhong, S. Hu, B. J. Liu, J. Y. Liu, C. Zong, Z. C. Lei, X. Wang, J. Aizpurua, R. Esteban and B. Ren, *Nat. Commun.*, 2017, **8**, 14891.

